Effective boundary conditions:
a general strategy and application to
compressible flows over rough boundaries

Giulia Deolmi, Wolfgang Dahmen and Siegfried Müller[*]

Institut für Geometrie und Praktische Mathematik
Templergraben 55, 52062 Aachen, Germany

*Corresponding author.
Email addresses: deolmi@igpm.rwth-aachen.de (G. Deolmi), dahmen@igpm.rwth-aachen.de (W. Dahmen),
mueller@igpm.rwth-aachen.de (S. Müller)

Effective boundary conditions: a general strategy and application to compressible flows over rough boundaries

Giulia Deolmi[1], Wolfgang Dahmen[1], and Siegfried Müller[1,*]

[1] *Institut für Geometrie und Praktische Mathematik, RWTH Aachen, Templergraben 55, 52056 Aachen, Germany.*

Abstract. Determining the drag of a flow over a rough surface is a guiding example for the need to take geometric micro-scale effects into account when computing a macro-scale quantity. A well-known strategy to avoid a prohibitively expensive numerical resolution of micro-scale structures is to capture the micro-scale effects through some *effective boundary conditions* posed for a problem on a (virtually) smooth domain. The central objective of this paper is to propose a "conceptual recipe" for the derivation of such effective boundary conditions first in a general setting of boundary value problems under the assumption of sufficient regularity to permit asymptotic expansions in terms of the micro-scale parameter. The proposed multiscale model relies then on an upscaling strategy based on homogenization techniques. It is similar in spirit to previous works by Achdou et al. [1], Jäger and Mikelic [29, 31], Friedmann et al. [24, 25] for incompressible fluids and Deolmi et al. [16, 17] for compressible fluids although with several noteworthy distinctions regarding e.g. the "micro-scale size" relative to boundary layer thickness or the systematic treatment of different boundary conditions. For proof of concept the general strategy is applied to the compressible Navier-Stokes equations to investigate steady, laminar, subsonic flow over a flat plate with partially embedded isotropic and anisotropic periodic roughness imposing adiabatic and isothermal wall conditions, respectively. The results are compared with high resolution simulations on a fully resolved rough domain.

AMS subject classifications: 74Q15, 76G25, 35Q30

Key words: Homogenization; upscaling strategy; effective boundary conditions; Navier wall law; compressible flow.

1 Introduction

From several scenarios in nature it is well-known that microstructures on surfaces can significantly reduce drag. For instance, the skin of a shark exhibits small-scale structures that makes the shark a very fast maritime hunter [59]. This has been confirmed by experiments conducted in oil channels to study biological surfaces, e.g., shark-skin replicas, hairy surfaces such as seal fur, [53–55], experiencing significant drag reduction. Such observations lead engineers to mimic this effect

---

Corresponding author. Email addresses: `deolmi@igpm.rwth-aachen.de` (G. Deolmi), `dahmen@igpm.rwth-aachen.de` (W. Dahmen), `mueller@igpm.rwth-aachen.de` (S. Müller)

for economical and ecological reasons in practical applications such as aviation. For instance, in [56, 57] riblets are shown to reduce the overall drag of airfoils and aircraft provided the riblet spacing is chosen appropriately. For flight tests of an Airbus 320 drag reduction was observed, see [58], but not as significant as for experiments in wind tunnels and oil channels, respectively. For a review on drag reduction using riblets we refer to [50–52].

To gain a deeper insight in the underlying physical mechanisms of drag reduction, simulations are performed that complement experimental investigations. Since resolving the microstructures requires a high resolution, numerical simulations are very expensive and, depending on the flow regime, are only feasible for small configurations. For a real application such as an airfoil the computational cost will be prohibitively high and a simulation will not be feasible in spite of an ever increasing computer power.

To deal with this type of problems a natural strategy is to resort to model reduction concepts such as *homogenization techniques* [10, 33, 48], *(heterogeneous) multiscale modeling* [21, 22] or multiscale finite element methods [20], that allow one to quantify the influence of small scale effects on the resolved macroscopic scale *without* directly resolving small scale structures. Typically, these concepts need to be adapted to the problem at hand, i.e., for a given concrete application the main task is to derive an appropriate upscaling strategy. It should be noted though that, strictly speaking, for the problems under consideration there is no clear (physical) scale separation so that a straightforward application of the heterogeneous multi-scale method is delicate. Rather the range of relevant scales is too large to be resolved.

Here we are particularly interested in an upscaling strategy where the micro-scale effect of a structured rough surface is modeled by means of effective boundary conditions given on a virtually smooth wall. For the derivation of these conditions the exact solution of the original problem on the rough domain is expanded in a *zeroth order solution* depending only on the macro-scale, i.e., the flow equations are solved in the artificial smooth domain, and an upscaling term that depends on macro-scale *and* micro-scale variables in order to capture the micro-scale effects suppressed in the zeroth order solution. A natural idea is to plug this ansatz into the original equation and try to see under which conditions low order terms cancel to eventually arrive at the so-called *cell problem* which is typically much simpler than the original problem. From the asymptotic expansion at an artificial smooth wall located on top of the roughness we can then deduce the *effective boundary conditions* [14] by means of a Taylor expansion in wall normal direction at the rough wall, where the mean of the solution of the cell problem enters as effective constant. Note that this differs from classical perturbation theory [37]. Finally, the effective problem is solved on the smooth domain with effective boundary conditions.

How this is carried out in concrete terms must depend on the specific problem and, in particular, on the type of the boundary conditions. In case of the steady incompressible Navier-Stokes equations this upscaling strategy has been developed and investigated by Achdou et al. [1] as well as Jäger and Mikelic [29, 31] for small Reynolds numbers. In [1] a Navier wall law is derived from a Taylor expansion of velocity and pressure where the zeroth order solution is first solved on an *extension* of the rough domain. These ideas are extended to unsteady problems in [2, 4, 7]. Applying an idea similar to [1] a Navier wall law is derived also in [12, 13] for the steady Poisson problem.

Some variations in the different approaches are perhaps worth pointing out. In contrast to Achdou et al., Jäger and Mikelic [29, 31] proceed differently. Instead of applying a Taylor expansion, a zeroth order approximation is computed first on a smooth *subset* of the rough domain and then it is continuously extended to the boundary of an effective domain with smooth boundary *overlapping* the roughness where it establishes the Navier wall law. Similar ideas are used in [27, 28, 30] to derive effective boundary conditions at the contact interface between a porous medium and a viscous incompressible fluid.

The methodology of Jäger and Mikelic is used in [23, 24] to solve a shape optimization problem, namely, finding the optimal "shape of the roughness" so as to minimize the drag force. Recently, this has been extended to turbulent incompressible flows, see [25]. Typically, only the influence in wall-normal direction is accounted for in the effective boundary conditions. This is justified as long as the flow is laminar. For instance, for turbulent flow the flow field is inherently three-dimensional and, thus, the roughness will most likely also affect the flow in streamwise and spanwise direction as well. In [25, 31], it is suggested to solve two cell problems, corresponding to the effects in streamwise and spanwise direction, respectively. For this purpose the flow at an oblique angle is considered on the macro-scale, introducing in this way the spanwise effects. However, no systematic strategy is given for the choice of the angle.

The aims pursued in the present paper are yet different in three major respects. First, we are particularly interested in *compressible* flows over a rough surface for high Reynolds numbers, which corresponds to considering a regime that significantly differs from the one analyzed in the aforementioned literature. In [16] we already derived a similar upscaling strategy combining ideas from Achdou et al. as well as Jäger and Mikelic. However, and this is the second delineating issue, we target a roughness scale relative to the viscous sublayer thickness which is *larger* than in those works because of significantly larger velocities. To account for this, the identification of the appropriate cell problem itself deserves some special attention. In order to make the underlying mechanisms transparent we outline first for a deliberately general scalar problem a systematic way - in some sense a "recipe" - for determining a suitable cell problem for the desired roughness range which is then used to identify effective boundary conditions. Targeting a roughness scale that is relatively large in comparison with the layer thickness in the compressible regime comes at a prize. Perhaps most importantly, in contrast to the aforementioned work, we need to account for the influence of the zeroth order solution in the cell problem and these terms can no longer be discarded. This causes several impediments. First, the cell problem becomes parameter-dependent. This has been verified already in [16] where computations for different cell problems have been carried out. For a detailed discussion on the differences between our model and the models of Achdou et al. as well as Jäger and Mikelic we refer to [16]. Second, the classical homogenization point of view passing the roughness scale to zero is perhaps not appropriate and one should rather look for quantitative effects for the targeted roughness range.

A completely rigorous foundation of our approach, as given in [28, 29] for a specific flow regime and in [36] for elliptic problems, is out of reach in the present framework. This brings us to the third point concerning the main objective of the present investigation, namely to develop *computationally viable* techniques for dealing with structured roughness for compressible flows, primarily focussing at this point on a numerical validation. The fact that the cell problem depends

on the zeroth order solution at a first glance seems to preclude its original purpose. However, the availability of certified model reduction techniques for exactly the type of problems arising as cell problems allows us to efficiently query the solution of the cell problem for many parameter values using reduced models. A second issue of practical relevance is how to acquire the information needed for the cell problem, namely the zeroth order solution. For simple geometries one can resort e.g. to van Driest's solution which avoids the computation of the zeroth order solution. Moreover, if the cell problem would be the only place where this information enters, such a qualitative approximation is expected to suffice. Therefore, as one option, we derive effective boundary conditions of *implicit* type confining knowledge about the zeroth order solution only in the cell problem which, as indicated above, can then be handled by reduced basis concepts.

In more complex situations a good guess about the zeroth order solution will generally be missing and this strategy is no longer viable. Our point of view then is that computing the zeroth order solution u^0 in a smooth domain on a reasonably coarse mesh is, in principle, affordable. We therefore discuss this as a second option leading to *explicit* effective boundary conditions. We test both variants of our approach highlighting, in particular, also the effect of different boundary conditions in the context of laminar compressible flows.

The paper is organized as follows: first, in Section 2 we outline sort of a general recipe for determining a suitable cell problem for various types of boundary conditions that comply with the above scale considerations for the roughness. In Section 3 we apply these considerations for an embedded periodic roughness to the compressible Navier-Stokes equations to investigate steady, laminar, subsonic flow of a perfect gas over an adiabatic and an isothermal wall, respectively. For proof of concept, in Section 4 we perform numerical simulations for isotropic and anisotropic periodic roughness. In Section 5 we summarize our results and conclude with an outlook on future work.

2   The Effective Problem - A General Strategy

In this section we present a guideline for the derivation of effective boundary conditions for problems involving boundaries with periodic roughness. We summarize the key ingredients and outline the steps that have to be performed in case of a concrete application. Starting point is the so-called *exact problem* defined on a *rough domain* $\Omega^\epsilon \subset \mathbb{R}^d$, $d = 2,3$, with boundary $\partial\Omega^\epsilon$ that is partly rough on $\Gamma_\epsilon \subset \partial\Omega^\epsilon$, see Figure 1(a):

$$\mathcal{L}(u^\epsilon) = 0 \quad \text{in} \quad \Omega^\epsilon, \tag{2.1a}$$

$$\mathcal{B}(u^\epsilon) = 0 \quad \text{on} \quad \Gamma_\epsilon, \tag{2.1b}$$

$$\overline{\mathcal{B}}(u^\epsilon) = 0 \quad \text{on} \quad \Gamma \subset \partial\Omega^\epsilon \backslash \Gamma_\epsilon. \tag{2.1c}$$

Here $\mathcal{L}$ and $\mathcal{B}$, $\overline{\mathcal{B}}$ denote a partial differential operator of order m, $m = 1,2$, and boundary value operators, respectively. In general, $\mathcal{L}$ will be nonlinear whereas $\mathcal{B}$ is assumed to be affine, for

instance, in case of Dirichlet or Neumann boundary conditions:

$$\mathcal{B}(u) := u - \overline{u}, \tag{2.2a}$$

$$\mathcal{B}(u) := \frac{\partial u}{\partial \boldsymbol{n}} - \overline{g}, \tag{2.2b}$$

where $\overline{u}$ and $\overline{g}$ are assumed to be constant functions. Depending on the type of the partial differential equation we have to impose additional boundary conditions on the remaining smooth boundary $\partial \Omega^{\epsilon} \backslash \Gamma_{\epsilon}$ or on parts of it. We assume that there exists a unique solution $u^{\epsilon} \in C^2(\Omega^{\epsilon}) \cap C^0(\overline{\Omega^{\epsilon}})$ to this boundary value problem.

(a) Rough domain Ω^{ϵ}.   (b) Smooth domain Ω^0.   (c) Effective domain Ω^{σ}.
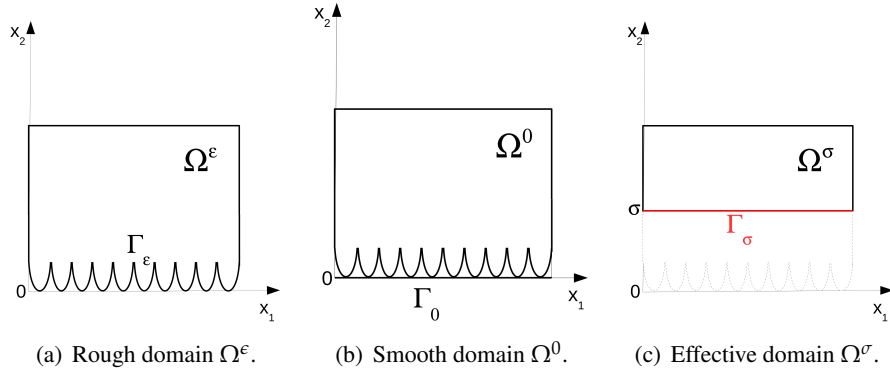
Figure 1: Domains on macro-scale.

For simplicity of presentation we will confine ourselves to a simple geometry Ω^{ϵ}, i.e., a rectangle ($d = 2$) and a hexahedron ($d = 3$), respectively, where the roughness is always located at the bottom. In addition we consider the domain $\Gamma_0 := \{ \boldsymbol{x} \in \Omega^0, \, x_2 = 0 \}$, which shares all boundary portions with Ω^{ϵ} except for the rough part which is replaced by its flat lower tangent Γ_0 so that $\Omega^{\epsilon} \subset \Omega^0$, as shown in Figure 1(b). The coordinates for these domains are referred to as *macro-scale variables* $\boldsymbol{x} \in \mathbb{R}^d$. Furthermore, the roughness is assumed to be periodic, i.e., Γ_{ϵ} is composed of periodic roughness elements, see Figure 2(a). These are referenced by discrete points $\bar{\boldsymbol{x}}_P \in \Gamma_0 \cap \Gamma_{\epsilon}$ and fixed periods $s_i^{L,R} > 0$, $s_i^{L,R} = \mathcal{O}(1)$, $i \neq 2$:

$$R(\bar{\boldsymbol{x}}_P) := \left\{ \boldsymbol{x} \in \Omega^{\epsilon}, \, x_i \in [\bar{x}_{P,i} - \epsilon s_i^L/2, \bar{x}_{P,i} + \epsilon s_i^R/2], \, i = 1, \ldots, d, \, i \neq 2 \right\}. \tag{2.3}$$

In what follows we assume for simplicity $s_i^L = s_i^R = s_i$ but emphasize that symmetry is not essential.

It will be crucial in what follows to relate the roughness elements $R(\bar{\boldsymbol{x}}_P)$ to a single reference *cell domain* Y with Lipschitz boundary ∂Y, defined by

$$Y := \times_{i=1, i \neq 2}^d (-s_i, s_i) \times \mathbb{R}_+, \tag{2.4}$$

where the factor $\mathbb{R}_+$ refers to the second coordinate y_2 of $\boldsymbol{y} \in Y$. Defining the mapping

$$\mathcal{Y}_{\bar{\boldsymbol{x}}_P} : R(\bar{\boldsymbol{x}}_P) \to Y: \quad \mathcal{Y}_{\bar{\boldsymbol{x}}_P}(\boldsymbol{x}) := \frac{\boldsymbol{x} - \bar{\boldsymbol{x}}_P}{\epsilon}, \quad \forall \boldsymbol{x} \in R(\bar{\boldsymbol{x}}_P), \tag{2.5}$$

each roughness element is then related to Y by $Y := \{ \boldsymbol{y} : \boldsymbol{y} = \mathcal{Y}_{\bar{\boldsymbol{x}}_P}(\boldsymbol{x}) \,,\, \boldsymbol{x} \in R(\bar{\boldsymbol{x}}_P) \}$, see 2(b).

Due to periodicity the cell domain serves as the same reference domain for all roughness elements.

(a) Roughness element $R(\bar{\boldsymbol{x}}_P)$.

(b) Cell domain Y.
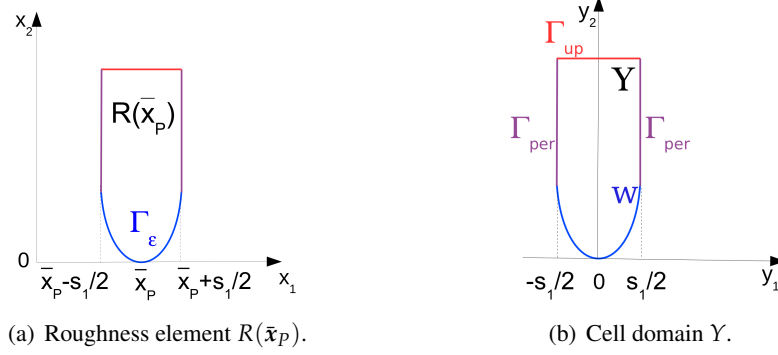
Figure 2: Roughness element in 2D: macro-scale and micro-scale.

Since solving the exact problem (2.1) numerically requires resolving the roughness by a discretization, the computational cost might be prohibitive. Therefore, it is of interest or sometimes mandatory to capture the effect of the roughness on the solution without resolving it by the discretization. This so-called *effective problem* is defined on an *effective domain* $\Omega^\sigma \subset \Omega^\epsilon$, see Figure 1(c), with smooth boundary $\Gamma_\sigma := \{ \boldsymbol{x} \in \Omega^\epsilon, \, x_2 = \sigma \}$ located on top of the roughness Γ_ϵ:

$$\mathcal{L}(u^{eff}) = 0 \quad \text{in} \quad \Omega^\sigma, \tag{2.6a}$$

$$\mathcal{B}^{eff}(u^{eff}) = 0 \quad \text{on} \quad \Gamma_\sigma \tag{2.6b}$$

$$\overline{\mathcal{B}}(u^{eff}) = 0 \quad \text{on} \quad \Gamma \subset \partial\Omega^\sigma \backslash \Gamma_\sigma \tag{2.6c}$$

In the effective problem we have to choose an appropriate boundary Γ_σ, i.e., $\sigma \geq \epsilon > 0$, and so-called *effective boundary conditions* $\mathcal{B}^{eff}$ defined on Γ_σ. In the following we will present a general strategy for the derivation of the effective problem that is motivated by but not restricted to the Navier-Stokes equations as in [1, 16, 24, 29]. Moreover, the ansatz for the upscaling differs to previous work resulting in a different cell problem.

For simplicity of presentation we consider first a scalar problem. The extension to systems is addressed at the end of the section.

Step 1: Asymptotic expansion Starting point is an asymptotic expansion of the solution u^ϵ of the exact problem (2.1) in terms of powers of ϵ whose existence in this form is at this point *assumed*:

$$u^\epsilon(\boldsymbol{x}) = u^0(\boldsymbol{x}) + \epsilon u^1(\boldsymbol{x}) + \epsilon^2 \theta\left(\boldsymbol{x}, \mathcal{Y}_{\bar{\boldsymbol{x}}_P}(\boldsymbol{x})\right), \tag{2.7}$$

where θ is a smooth function. The validity of this expansion is assumed for any $\boldsymbol{x} \in R(\bar{\boldsymbol{x}}_P) \subset \Omega^\epsilon$ close to the rough surface, i.e., $\text{dist}(\boldsymbol{x}, \Gamma_\epsilon) \ll 1$. Here u^0 denotes the solution of the *zeroth order*

problem

$$\mathcal{L}(u^0) = 0 \quad \text{in} \quad \Omega^0, \tag{2.8a}$$

$$\mathcal{B}(u^0) = 0 \quad \text{on} \quad \Gamma_0, \tag{2.8b}$$

$$\overline{\mathcal{B}}(u^0) = 0 \quad \text{on} \quad \Gamma \subset \partial\Omega^0 \backslash \Gamma_0, \tag{2.8c}$$

posed on the smooth domain Ω^0, which corresponds to the formal limit of vanishing roughness.

Step 2: Ansatz for the upscaling function u^1. Of course, the expansion (2.7) does not pin down u^1 and any perturbation of order $O(\epsilon)$ would be admissible. We try to exploit this ambiguity as follows. In contrast to classical perturbation theory [37], we *assume* at this point that the *upscaling function* u^1 depends on *both* the macro-scale variable x and the micro-scale variable $y(x) = (x - \bar{x}_P)/\epsilon$ and in compliance with (2.7) can be represented as

$$u^1(x) = \beta(\mathcal{Y}_{\bar{x}_P}(x)), \quad x \in R(\bar{x}_P), \bar{x}_P \in \Gamma_0, \tag{2.9}$$

where the so-called *cell function* $\beta(y)$ is assumed to be a sufficiently smooth function of the variable y in the (reference-)cell domain Y. Thus, the dependence of u^1 on x is assumed to be only through the mapping $\mathcal{Y}_{\bar{x}_P}: x \in R(\bar{x}_P) \to Y$. Moreover, as will be seen later, the cell function β depends in general on macro-scale quantities which may depend also on the spatial location of the respective roughness element. Whenever this dependence matters we write $\beta(\cdot) = \beta_{\bar{x}_P}(\cdot)$. When there is no risk of confusion we sometimes suppress the reference to the particular roughness element and in fact almost always suppress the subscript $\bar{x}_P$. We emphasize that in the literature, see [2, 23, 28], one finds the particular choice

$$\beta(\mathcal{Y}_{\bar{x}_P}(x)) = \frac{\partial u^0}{\partial x_2}(\bar{x}_P)(\mathcal{Y}_{\bar{x}_P}(x) \cdot e_2), \tag{2.10}$$

whereas our approach is closer to classical homogenization techniques, see [10, 45].

Step 3: Derivation of closing conditions We now have to find appropriate closing conditions such that the expansion (2.7) holds. For this purpose, we proceed in two steps where we consider $x \in R(\bar{x}_P) \subset \Omega^\epsilon$ and $x \in R(\bar{x}_P) \cap \Gamma_\epsilon$, respectively.

Step 3a: Partial differential equations. We consider first the case that $\mathcal{L}$ contains only derivatives of equal order m. Given u^0 we wish to find u^1 of the form (2.9) and β, respectively, such that

$$\mathcal{L}\left(u^0 + \epsilon\beta(\mathcal{Y}_{\bar{x}_P}(\cdot)) + \epsilon^2\theta(\cdot, \mathcal{Y}_{\bar{x}_P}(\cdot))\right)(x) = 0, \quad x \in R(\bar{x}_P), \tag{2.11}$$

which is, of course, only determined modulo an $O(\epsilon^2)$ term which we do not know. Discarding all terms of order $\mathcal{O}(\epsilon^{2-m})$ when expanding the left-hand side of (2.11), which corresponds to discarding $O(\epsilon^2)$ terms in the argument, and taking into account that the derivatives of the upscaling

function with respect to the macro-scale variable read

$$\frac{\partial^{\boldsymbol{i}} u^1}{\partial x^{\boldsymbol{i}}}(\boldsymbol{x}) = \frac{1}{\epsilon^{|\boldsymbol{i}|}} \frac{\partial^{\boldsymbol{i}} \beta}{\partial y^{\boldsymbol{i}}}(\mathcal{Y}_{\bar{\boldsymbol{x}}_P}(\boldsymbol{x})), \quad \boldsymbol{x} \in R(\bar{\boldsymbol{x}}_P),$$

$\boldsymbol{i} \in \mathbb{N}_0^d$, $|\boldsymbol{i}| := \sum_{k=1}^d i_k \leq m$, we obtain an expression of the form

$$\mathcal{C}(\beta)(\mathcal{Y}_{\bar{\boldsymbol{x}}_P}(\boldsymbol{x})) = \mathcal{O}(\epsilon^{2-m}), \quad \boldsymbol{x} \in R(\bar{\boldsymbol{x}}_P). \tag{2.12}$$

This relation depends, of course, on the operator $\mathcal{L}$ as well as on the zeroth order solution $u^0|_{R(\bar{\boldsymbol{x}}_P)}$ restricted to the particular $R(\bar{\boldsymbol{x}}_P)$ and implicitly on the reference point $\bar{\boldsymbol{x}}_P \in \Gamma_\epsilon \cap \Gamma_0$ through the mapping $\mathcal{Y}_{\bar{\boldsymbol{x}}_P}$. The important point for us though is the fact that (2.12) can be obviously rephrased as a relation formulated in terms of the micro-scale variable $\boldsymbol{y} = \mathcal{Y}_{\bar{\boldsymbol{x}}_P}(\cdot)$. Moreover, since we cannot identify the $\mathcal{O}(\epsilon^{2-m})$ terms we seek to determine the field β through

$$\mathcal{C}_{\mathcal{L},\bar{\boldsymbol{x}}_P,u^0}(\beta)(\boldsymbol{y}) = \mathcal{C}(\beta)(\boldsymbol{y}) = \mathcal{C}(\boldsymbol{y}) = 0, \quad \boldsymbol{y} \in Y. \tag{2.13}$$

We list the various notational versions to indicate that we suppress at times, if there is no risk of confusion, some or all subscripts, and even β, in favor of a less cluttered notation. We refer to $\mathcal{C} = \mathcal{C}_{\mathcal{L},\bar{\boldsymbol{x}}_P,u^0}$ as the *cell operator* acting on an unknown field β as a function of the micro-scale variable $\boldsymbol{y}$.

For instance, in case of the linear Laplace operator $\mathcal{L}(u) = \Delta u$, the nonlinear transport operator $\mathcal{L}(u) = (u,\ldots,u) \cdot \nabla u$ or the nonlinear operator $\mathcal{L}(u) = \nabla u \cdot \nabla u$ we obtain (suppressing the dependence on $\bar{\boldsymbol{x}}_P$ and u^0 in the notation)

$$\mathcal{C}_\Delta(\boldsymbol{y}) = \left(\frac{1}{\epsilon} \sum_{i=1}^d \frac{\partial^2 \beta}{\partial y_i^2}(\boldsymbol{y}) \right) \tag{2.14}$$

$$\mathcal{C}_\nabla(\boldsymbol{y}) = \left(u^0(\mathcal{Y}_{\bar{\boldsymbol{x}}_P}^{-1}(\cdot)) \sum_{i=1}^d \frac{\partial \beta}{\partial y_i}(\boldsymbol{y}) \right) \tag{2.15}$$

$$\mathcal{C}_{\nabla^2}(\boldsymbol{y}) = 2\sum_{i=1}^d \frac{\partial u^0}{\partial x_i}(\mathcal{Y}_{\bar{\boldsymbol{x}}_P}^{-1}(\cdot)) \frac{\partial \beta}{\partial y_i}(\boldsymbol{y}) + \sum_{i=1}^d \left(\frac{\partial \beta}{\partial y_i}(\boldsymbol{y}) \right)^2,$$

respectively.

If $\mathcal{L} = \sum_{i=1}^m \mathcal{L}_i$ is the sum of operators $\mathcal{L}_i$, such that each term in $\mathcal{L}_i$ is homogeneous of order i, we introduce for each operator $\mathcal{L}_i$ a cell operator $\mathcal{C}_i$ according to (2.12). Then $\mathcal{C}$ in (2.12) is the sum of $\mathcal{C}_i$. Analogously to (2.12), we then approximate each cell operator separately by discarding the terms of order $\mathcal{O}(\epsilon^{2-i})$

$$\mathcal{C}_{i,\bar{\boldsymbol{x}}_P,u^0}(\beta)(\boldsymbol{y}) = \mathcal{L}_i(u^\epsilon)(\mathcal{Y}_{\bar{\boldsymbol{x}}_P}^{-1}(\boldsymbol{y})) + \mathcal{O}(\epsilon^{2-i}). \tag{2.16}$$

Then $\mathcal{C}$ in (2.13) is given by the sum of the $\mathcal{C}_i$, obtained by discarding $\mathcal{O}(\epsilon^{2-i})$ terms.

For instance, in case of the linear operator $\mathcal{L}(u) = \eta \Delta u + \boldsymbol{\alpha} \cdot \nabla u$ we obtain

$$\mathcal{C}_{\mathcal{L}}(\beta)(\boldsymbol{y}) = \frac{\eta}{\epsilon} \sum_{i=1}^d \frac{\partial^2 \beta}{\partial y_i^2}(\boldsymbol{y}) + \alpha_i \frac{\partial \beta}{\partial y_i}(\boldsymbol{y}), \quad \boldsymbol{y} \in Y = \mathcal{Y}_{\bar{\boldsymbol{x}}_P}(R(\bar{\boldsymbol{x}}_P)). \tag{2.17}$$

As we can conclude from the examples (2.14), (2.15), (2.16) and (2.17), the cell operator $\mathcal{C}_{\mathcal{L}}$ is in general nonlinear but may be linear even for nonlinear operators $\mathcal{L}$, cf. (2.15).

Step 3b: Boundary conditions. To derive boundary conditions for the cell function β on the boundary portion W of ∂Y, we proceed in analogy to (2.12) and seek a *boundary cell operator* $\mathcal{C}_{\mathcal{B}}$ acting on β which satisfies

$$\mathcal{C}_{\mathcal{B},\bar{\boldsymbol{x}}_P,u^0}(\beta)(\boldsymbol{y}) = \mathcal{B}\left(u^0(\mathcal{Y}_{\bar{\boldsymbol{x}}_P}^{-1}(\boldsymbol{y})) + \epsilon u^1(\mathcal{Y}_{\bar{\boldsymbol{x}}_P}^{-1}(\boldsymbol{y})) + \epsilon^2\theta(\mathcal{Y}_{\bar{\boldsymbol{x}}_P}^{-1}(\boldsymbol{y}),\boldsymbol{y})\right) + \mathcal{O}(\epsilon^{2-m_{\mathcal{B}}}), \quad (2.18)$$

when $m_{\mathcal{B}}$ is the (homogeneous) order of the boundary operator $\mathcal{B}$, i.e., $m_{\mathcal{B}} = 0$ for a pure Dirichlet condition and $m_{\mathcal{B}} = 1$ in the Neumann case. We then impose conditions on β by requiring that

$$\mathcal{C}_{\mathcal{B},\bar{\boldsymbol{x}}_P,u^0}(\beta)(\boldsymbol{y}) = \mathcal{C}_{\mathcal{B}}(\beta)(\boldsymbol{y}) = \mathcal{C}(\beta)(\boldsymbol{y}) = 0, \quad \boldsymbol{y} \in W = \mathcal{Y}_{\bar{\boldsymbol{x}}_P}(\Gamma_\epsilon \cap R(\bar{\boldsymbol{x}}_P)), \quad (2.19)$$

where our earlier comments on the use of subscripts apply here as well.

In the case of Dirichlet conditions $\mathcal{B}(u) = u - \bar{u}$ (see (2.2a)) on Γ_ϵ, with $\bar{u} \equiv const$, we have for $\boldsymbol{x} \in \Gamma_\epsilon \cap R(\bar{\boldsymbol{x}}_P)$, taking $u^0(\bar{\boldsymbol{x}}_P) = \bar{u}$ into account,

$$\begin{aligned} \mathcal{C}_{Dir}(\beta)(\mathcal{Y}_{\bar{\boldsymbol{x}}_P}(\boldsymbol{x})) &= u^0(\boldsymbol{x}) + \epsilon\beta(\mathcal{Y}_{\bar{\boldsymbol{x}}_P}(\boldsymbol{x})) + \epsilon^2\theta(\mathcal{Y}_{\bar{\boldsymbol{x}}_P}(\boldsymbol{x})) - \bar{u} \\ &= (\boldsymbol{x} - \bar{\boldsymbol{x}}_P) \cdot \nabla u^0(\bar{\boldsymbol{x}}_P) + \epsilon\beta(\mathcal{Y}_{\bar{\boldsymbol{x}}_P}(\boldsymbol{x})) + O(\epsilon^2), \quad \boldsymbol{x} \in \Gamma_\epsilon \cap R(\bar{\boldsymbol{x}}_P). \end{aligned}$$

Thus, on the cell Y (2.19) takes the form

$$\mathcal{C}_{Dir,\bar{\boldsymbol{x}}_P,u^0}(\beta)(\boldsymbol{y}) := \boldsymbol{y} \cdot \nabla u^0(\bar{\boldsymbol{x}}_P) + \beta(\boldsymbol{y}) = 0, \quad \boldsymbol{y} \in W. \quad (2.20)$$

Analogously we can proceed for the Neumann conditions $\partial_n u(\boldsymbol{x}) = \bar{g}$ on Γ_ϵ to obtain for $\boldsymbol{x} \in \Gamma_\epsilon \cap R(\bar{\boldsymbol{x}}_P)$

$$\mathcal{B}(u^\epsilon)(\boldsymbol{x}) = \partial_n u^0(\boldsymbol{x}) - \bar{g} + \boldsymbol{n}_\epsilon(\boldsymbol{x})^T \nabla_y \beta(\mathcal{Y}_{\bar{\boldsymbol{x}}_P}(\boldsymbol{x})) + O(\epsilon),$$

where $\boldsymbol{n}_\epsilon(\boldsymbol{x})$ denotes the outward normal at $\boldsymbol{x} \in \Gamma_\epsilon$. Taking $\partial_n u(\bar{\boldsymbol{x}}_P) = \bar{g}$ into account in the expansion

$$\begin{aligned} \partial_n u^0(\boldsymbol{x}) - \bar{g} &= \partial_n u^0(\bar{\boldsymbol{x}}_P) - \bar{g} \\ &\quad + (\boldsymbol{x} - \bar{\boldsymbol{x}}_P) \cdot \nabla(\partial_n u^0)(\bar{\boldsymbol{x}}_P) + O(|\boldsymbol{x} - \bar{\boldsymbol{x}}_P|^2) \\ &= (\boldsymbol{x} - \bar{\boldsymbol{x}}_P) \cdot \nabla(\partial_n u^0)(\bar{\boldsymbol{x}}_P) + O(|\boldsymbol{x} - \bar{\boldsymbol{x}}_P|^2), \end{aligned}$$

recalling that we can discard terms of order $O(\epsilon)$, and denoting $\boldsymbol{n}(\boldsymbol{y}) = \boldsymbol{n}_\epsilon(\bar{\boldsymbol{x}}_P + \epsilon\boldsymbol{y})$ for $\boldsymbol{y} \in W \subset \partial Y$ corresponding to $\boldsymbol{x} \in \Gamma_\epsilon \cap R(\bar{\boldsymbol{x}}_P)$, we are led to define

$$\mathcal{C}_{Neu}(\beta)(\boldsymbol{y}) := \boldsymbol{n}(\boldsymbol{y})^T \nabla_y \beta(\boldsymbol{y}), \quad \boldsymbol{y} \in W. \quad (2.21)$$

In summary, the boundary conditions for the cell function β take the following form

$$\mathcal{C}_{\mathcal{B},\bar{\boldsymbol{x}}_P,u^0}(\beta)(\boldsymbol{y}) = 0, \quad \boldsymbol{y} \in W. \quad (2.22)$$

Step 3c: Cell problem. We are now prepared to formulate the cell problem and recall the periodicity of the roughness in streamwise direction. Subdividing the cells in streamwise direction, it is natural to impose periodicity constraints in this direction as well, since the dependence of the upscaling functions on the location in streamwise direction is guaranteed through the dependence on u^0. Since the solution of the cell problem is expected to converge fast in the y_2-direction we also impose homogeneous Neumann conditions on Γ_{up} opposite to W, see Figure 2(b).

The *cell problem* on the cell domain Y reads now as follows

$$\mathcal{C}_{\mathcal{L}}(\beta)(y) = \mathcal{C}_{\mathcal{L}, \bar{x}_P, u^0}(\beta)(y) = 0, \quad \text{in} \quad Y, \tag{2.23a}$$

$$\mathcal{C}_{\mathcal{B}}(\beta)(y) = \mathcal{C}_{\mathcal{B}, \bar{x}_P, u^0}(\beta)(y) = 0, \quad \text{on} \quad W, \tag{2.23b}$$

$$\frac{\partial \beta}{\partial n^y} = 0, \quad \text{on} \quad \Gamma_{up}, \tag{2.23c}$$

$$y_i - \text{periodic}, \ i \neq 2. \tag{2.23d}$$

The actual solvability of the cell problem needs to be discussed for a given concrete application.

Anticipating the numerical results shown later below we expect that the cell functions converge to some constant value for $y_2 \to \infty$. Therefore, we make the following assumption:

Hypothesis: 2.1. (I) The normal slope of the cell function tends to zero when $y_2 \to \infty$, faster than linearly, i.e.,

$$\lim_{y_2 \to \infty} y_2 \left\| \frac{\partial \beta(\cdot, y_2)}{\partial y_2} \right\|_{L_\infty(-s,s)} = 0. \tag{2.24}$$

(II) The cell function β converges uniformly to a constant for $y_2 \to \infty$, i.e., there exists a b such that

$$\lim_{y_2 \to \infty} \|\beta|_{\Gamma_{up}^{y_2}} - b\|_\infty = 0. \tag{2.25}$$

Remark 2.1. Defining the y_2-cross sections $\Gamma_{up}^{y_2} := \{\overline{y} \in Y : \overline{y}_2 = y_2\}$ with $y_2 \geq 1$, along with the corresponding means

$$\langle \beta \rangle (y_2) := \frac{1}{|\Gamma_{up}^{y_2}|} \int_{\Gamma_{up}^{y_2}} \beta d\gamma,$$

(II) implies that $b = \lim_{y_2 \to \infty} \langle \beta \rangle (y_2)$. Moreover, we infer from (I) that

$$\frac{y_2 \partial \langle \beta \rangle (y_2)}{\partial y_2} \to 0, \quad y_2 \to \infty. \tag{2.26}$$

For the Poisson problem the convergence (I), (II) can actually be shown to be even exponential. As in [16], numerical computations confirm that the effective constant is actually independent of the y_2-cross-sections $\Gamma_{up}^{y_2}$ for $y_2 \geq 1$, i.e., $\langle \beta \rangle (y_2) = \langle \beta \rangle := b$ which in the specific applications below can be shown rigorously.

Step 4: Effective boundary conditions. We emphasize that the zeroth order function u^0 and its derivatives enter as parameters in the cell problem (2.23), whereas in the literature, see e.g. [1–4, 27–31], the cell problem is solved only once without involving any reference to u^0. For our applications, one cannot avoid the dependence on u^0 in the target range for the roughness scale, cf. [16]. Nevertheless, we can save most of the benefit of such an upscaling strategy in the envisaged applications corresponding to the following two application scenarios:

ApplSc.1: We assume that u^0 and ∇u^0 do not exhibit significant variations over the rough portion of Γ_ϵ and that we have a good estimate for u^0 and for $\nabla u^0(\bar{x}_P)$ for each reference point $\bar{x}_P$ at hand. For instance, for a compressible flow in a simple domain geometry van Driest's solution may serve that purpose (see the later numerical experiments). In this case we wish to *avoid* computing the field u^0 numerically.

ApplSc.2: In general an appropriate guess for u^0 and $\nabla u^0(\bar{x}_P)$ will be lacking. In this case the quantities u^0 and $\nabla u^0(\bar{x}_P)$ need to be computed numerically. The rationale of the proposed approach is then that it still pays to trade two flow solves on simple smooth domains (the one for u^0 possibly even with a coarser mesh) against a single solve with *resolved* geometric microstructures. In this case this information is used in the cell problem and for formulating the effective boundary conditions.

We determine next the effective boundary conditions $\mathcal{B}^{eff}$ in (2.6b) for both scenarios. Here we confine ourselves to two cases where for the exact problem (2.1) and the zeroth order problem (2.8) we have Dirichlet or Neumann boundary conditions, see (2.2a) and (2.2b), respectively. Regarding the significance of the following considerations in the present generality a note of caution is in order since the sensitivity of boundary conditions under perturbations depends on the concrete case at hand. To see what could be said as a general guideline, in order to derive the effective boundary conditions we investigate the solution u^ϵ of the exact problem on Γ_σ.

Step 4a - Dirichlet case: In the following Γ_σ denotes a plane offset of Γ_0 at the position $\sigma \mathbf{e}_2$ above Γ_ϵ and assume that $\sigma = \mathcal{O}(\epsilon)$, so that $\|x - \bar{x}_P\| = \mathcal{O}(\epsilon)$ for $x \in \Gamma_\sigma$.

ApplSc.1: As a first step a Taylor expansion of u^0 at $x \in \Gamma_\sigma \cap R(\bar{x}_P)$ around $\bar{x}_P \in \Gamma_0$ yields

$$u^0(x) = u^0(\bar{x}_P) + \epsilon \sum_{j=1}^d \frac{\partial u^0}{\partial x_j}(\bar{x}_P) \frac{x_j - \bar{x}_{P,j}}{\epsilon} + \mathcal{O}(\|x - \bar{x}_P\|^2) \ .$$

Inserting the Taylor expansion into the expansion (2.7) and using (2.9), we obtain

$$
\begin{aligned}
u^\epsilon(x) &= u^0(x) + \epsilon u^1(x) + \mathcal{O}(\epsilon^2) \\
&= u^0(x) + \epsilon \beta(\mathcal{Y}_{\bar{x}_P}(x)) + \mathcal{O}(\epsilon^2) \\
&= u^0(\bar{x}_P) + \sum_{j=1}^d \frac{\partial u^0}{\partial x_j}(\bar{x}_P)(x_j - \bar{x}_{P,j}) + \epsilon \beta(\mathcal{Y}_{\bar{x}_P}(x)) + \mathcal{O}(\epsilon^2).
\end{aligned}
\tag{2.27}
$$

Using the Dirichlet conditions at $\bar{x}_P \in \Gamma_0$, we rewrite (2.27) as

$$u^\epsilon(x) = \bar{u} + \epsilon \nabla u^0(\bar{x}_P) \cdot \mathcal{Y}_{\bar{x}_P}(x) + \epsilon \beta(\mathcal{Y}_{\bar{x}_P}(x)) + \mathcal{O}(\epsilon^2). \tag{2.28}$$

The rationale of formulating next *effective boundary conditions* is to realize the right-hand side of (2.28) on Γ_σ by effectively computable quantities, ideally up to an error of $O(\epsilon^2)$. Specifically, note that $y_2 = \sigma/\epsilon$ for $y = \mathcal{Y}_{\bar{x}_P}(x), x \in \Gamma_\sigma \cap R(\bar{x}_P)$. Moreover, β deviates from its mean on Γ_σ only by a very small amount and the wall-normal derivative of the effective flow at $\bar{x}_P$ should be close to that of u^0.

In order to avoid the explicit use of $\nabla u^0(\bar{x}_P)$ in the boundary conditions, we formulate the following *implicit effective boundary conditions*

$$u^{eff}(x) - \epsilon \sum_{j \in \mathcal{J}_\mathcal{D}} \frac{\partial u^{eff}}{\partial x_j}(x)(\mathcal{Y}_{\bar{x}_P}(x)) = \bar{u}(x) + \epsilon \langle \beta \rangle, \quad x \in R(\bar{x}_P), \quad \mathcal{C}_{\mathcal{L}, \bar{x}_P, u^0}(\beta) = 0, \tag{2.29}$$

where we set $\mathcal{J}_\mathcal{D} := \{ j \in \{1, \ldots, d\} \text{ s.t. } \partial u^0/\partial x_j(\bar{x}_P) \neq 0 \}$. Observe that (2.29) is in fact of Robin type. One expects this to weaken somewhat the influence of a possible spatial variation of the field u^0 which now enters only through the cell function β that solves an equation depending on $\bar{x}_P$.

ApplSc.2: Inserting (2.9) into the expansion (2.7), for $x \in \Gamma_\sigma \cap R(\bar{x}_P)$ we obtain

$$u^\epsilon(x) = u^0(x) + \epsilon u^1(x) + \mathcal{O}(\epsilon^2) = u^0(x) + \epsilon \beta(\mathcal{Y}_{\bar{x}_P}(x)) + \mathcal{O}(\epsilon^2).$$

In this case we make explicit use of $u^0(x)$ also in the boundary conditions and set

$$u^{eff}(x) = u^0(x) + \epsilon \langle \beta \rangle, \quad x \in R(\bar{x}_P), \tag{2.30}$$

which is an *explicit Dirichlet condition*.

Step 4b: Neumann case. In this case we proceed similarly where we consider the derivative of u^ϵ instead of the function u^ϵ. The ansatz (2.7) yields

$$\frac{\partial u^\epsilon}{\partial n^\sigma}(x) = \frac{\partial u^0}{\partial n^\sigma}(x) + \epsilon \frac{\partial u^1}{\partial n^\sigma}(x) + \epsilon^2 \frac{\partial}{\partial n^\sigma} \theta(x, \mathcal{Y}_{\bar{x}_P}(x)) \tag{2.31}$$

for any point $x \in \Gamma_\sigma \cap R(\bar{x}_P)$, where $n^\sigma(x) = e_2$ denotes the normal to Γ_σ at x.

For the second term on the right-hand side in (2.31) we derive from (2.9)

$$\frac{\partial u^1}{\partial n^\sigma}(x) = \frac{\partial u^1}{\partial x_2}(x) = \frac{1}{\epsilon} \frac{\partial \beta}{\partial y_2}(\mathcal{Y}_{\bar{x}_P}(x)), \quad x \in \Gamma_\sigma \cap R(\bar{x}_P). \tag{2.32}$$

ApplSc.1. Again, a Taylor expansion provides

$$\frac{\partial u^0}{\partial n^\sigma}(x) = \frac{\partial u^0}{\partial x_2}(x) = \frac{\partial u^0}{\partial x_2}(\bar{x}_P) + \sum_{j=1}^{d} \frac{\partial^2 u^0}{\partial x_2 \partial x_j}(\bar{x}_P)(x_j - \bar{x}_{P,j}) + \mathcal{O}(\epsilon^2). \tag{2.33}$$

Inserting (2.33) and (2.32) into the right-hand side of (2.31) and using the boundary condition (2.8b), we obtain

$$\frac{\partial u^\epsilon}{\partial n^\sigma}(x) = \bar{g} + \frac{\partial \beta}{\partial y_2}(\mathcal{Y}_{\bar{x}_P}(x)) + \epsilon \sum_{j=1}^{N} \frac{\partial^2 u^0}{\partial x_2 \partial x_j}(\bar{x}_P)(\mathcal{Y}_{\bar{x}_P}(x))_j + \epsilon^2 \frac{\partial}{\partial n^\sigma}\theta(x, \mathcal{Y}_{\bar{x}_P}(x)) + \mathcal{O}(\epsilon^2) .$$

(2.34)

We recall that $y_2 = \sigma/\epsilon$.

Unfortunately, we do not know the fourth summand on the right-hand side of (2.34). So, in formulating effective Neumann conditions, all we can do is to incorporate the corrective effect of those terms we know. As we will see later on in the numerical results, this approximation is indeed not as accurate as in the Dirichlet case.

In **ApplSc.1** we wish to avoid using the quantities $\frac{\partial^2 u^0}{\partial x_i \partial x_j}(\bar{x}_P)$ and formulate therefore the *implicit boundary condition*

$$\frac{\partial u^{eff}}{\partial n^\sigma}(x) \;=\; \bar{g} + \frac{\partial \langle \beta \rangle}{\partial y_2} + \epsilon \sum_{j \in \mathcal{J}_N} \frac{\partial^2 u^{eff}}{\partial x_2 \partial x_j}(x)(\mathcal{Y}_{\bar{x}_P}(x))_j, \quad x \in \Gamma_\sigma \cap R(\bar{x}_P),$$

to hold on Γ_σ, where $\mathcal{J}_N := \{ j \in \{1, \dots, d\}, \text{ s.t. } \partial^2 u^0/\partial x_2 \partial x_j(\bar{x}_P) \neq 0 \}$. Note that, by (2.26), the mean $\langle \beta \rangle (y_2)$ hardly depends on the choice of Γ_{up}, i.e., the term $\frac{\partial}{\partial y_2}\langle \beta \rangle$ is expected to be very small which, in turn, motivates imposing only

$$\frac{\partial u^{eff}}{\partial n^\sigma}(x) \;=\; \bar{g} + \epsilon \sum_{j \in \mathcal{J}_N} \frac{\partial^2 u^{eff}}{\partial x_2 \partial x_j}(x)(\mathcal{Y}_{\bar{x}_P}(x))_j, \quad x \in \Gamma_\sigma \cap R(\bar{x}_P)$$

(2.35)

on Γ_σ.

ApplSc.2. If good estimates for $\frac{\partial u^0}{\partial x_j}(x)$ are available, from equation (2.31), we derive the *explicit boundary condition*

$$\frac{\partial u^{eff}}{\partial n^\sigma}(x) \;=\; \frac{\partial u^0}{\partial n^\sigma}(x) + \frac{\partial \langle \beta \rangle}{\partial y_2}, \quad x \in \Gamma_\sigma \cap R(\bar{x}_P)$$

again with the option of discarding the second term on the right-hand side, i.e.

$$\frac{\partial u^{eff}}{\partial n^\sigma}(x) \;=\; \frac{\partial u^0}{\partial n^\sigma}(x), \quad x \in \Gamma_\sigma.$$

(2.36)

Step 5: Choice of σ. It remains to specify the parameter σ subject to the conditions $\sigma \geq \epsilon$ and $\sigma = \mathcal{O}(\epsilon)$. A natural idea is to choose σ so as to minimize the deviation of u^ϵ and u^{eff} on Γ_σ. For the implicit version of the effective Dirichlet boundary consitions we deduce from (2.28) and (2.29) that

$$u^\epsilon(x) - u^{eff}(x) \;=\; \epsilon\big(\beta(\mathcal{Y}_{\bar{x}_P}(x)) - \langle \beta \rangle\big)$$
$$+ \epsilon \sum_{j \in \mathcal{J}_D} \left(\frac{\partial u^0}{\partial x_j}(\bar{x}_P) - \frac{\partial u^{eff}}{\partial x_j}(x) \right)(\mathcal{Y}_{\bar{x}_P}(x))_j + \mathcal{O}(\epsilon^2)$$

(2.37)

for any point $x \in \Gamma_\sigma \cap R(\bar{x}_P)$. Recall that $y_2 = \sigma/\epsilon$. Choosing σ large will diminish the first sum because of the convergence of $\beta(\cdot, y_2, \cdot)$ towards its mean. The second sum, in turn, is expected to have a smaller contribution for y_2 (and hence σ) smaller because closer to Γ_ϵ the deviation between u^{eff} and u^0 should be smaller. One could consider optimizing σ via a posteriori information but for simplicity we take here the smallest admissible value of σ namely

$$\sigma = \epsilon . \tag{2.38}$$

For *explicit* effective boundary conditions we obtain

$$u^\epsilon(x) - u^{eff}(x) = \epsilon \big(\beta(\mathcal{Y}_{\bar{x}_P}(x)) - \langle \beta \rangle \big) + \mathcal{O}(\epsilon^2), \quad x \in \Gamma_\sigma \cap R(\bar{x}_P), \tag{2.39}$$

which, by Hypothesis 2.1, gives rise essentially to an $\mathcal{O}(\epsilon^2)$ error for $\sigma = k\epsilon$, when k tends to infinity. Since we do not know a priori how fast $\beta(\mathcal{Y}_{\bar{x}_P}(x))$ converges to $\langle \beta \rangle$, we use the choice (2.38) also in the *explicit* case.

As one may expect from the higher sensitivity of Neumann data, it is less clear how to draw analogous conclusions in the Neumann case. As a rough indication we inspect the deviation of the respective fluxes on Γ_σ. To that end, we deduce from (2.34) and (2.35) for *implicit* effective boundary conditions

$$\frac{\partial u^\epsilon}{\partial n^\sigma}(x) - \frac{\partial u^{eff}}{\partial n^\sigma}(x) = \tag{2.40}$$
$$\frac{\partial \beta}{\partial y_2}(\mathcal{Y}_{\bar{x}_P}(x)) + \epsilon \sum_{j \in \mathcal{J}_N} y_j(x) \left(\frac{\partial^2 u^0}{\partial x_2 \partial x_j}(\bar{x}_P) - \frac{\partial^2 u^{eff}}{\partial x_2 \partial x_j}(x) \right) + \epsilon^2 \frac{\partial}{\partial n^\sigma} \theta(x, \mathcal{Y}_{\bar{x}_P}(x)).$$

Again, the first summand is expected to be negligible because of the convergence of the fields β in wall normal direction (see Hypothesis 2.1) and would therefore benefit from a larger σ while the second summand is expected to exhibit the opposite effect. Therefore, we retain the choice (2.38).

For *explicit* effective boundary conditions the second term on the right-hand side of (2.40) drops out.

So far the mechanisms reflected by the previous five steps refer to a scalar problem. In principle, except for the global role of the boundary conditions, the previous steps can be formulated component-wise where we replace the scalars u^ϵ, u^0 and u^1 by vectors of K components, i.e., $u^\epsilon = (u_1^\epsilon, \ldots, u_K^\epsilon)$, $u^0 = (u_1^0, \ldots, u_K^0)$ and $u^1 = (u_1^1, \ldots, u_K^1)$. For each cell function u_i^1 we introduce an own cell function β_i, i.e., in (2.9) we have

$$u_i^1(x) = \beta_i(\mathcal{Y}_{\bar{x}_P}(x)), \quad x \in R(\bar{x}_P), \bar{x}_P \in \Gamma_0 . \tag{2.41}$$

This differs from previous work [1, 16, 24, 29] mainly because of a different target range for the roughness ϵ which leads to formulating the cell problem (2.23) by Step 3. Here we assume that Dirichlet and Neuman boundary conditions apply to separate quantities, i.e., for each variable u_i we have either Dirichlet or Neumann conditions that do not depend on the other variables.

2.1 Approximation of $\langle \beta_{\bar{\boldsymbol{x}}_P} \rangle$

As previously described, in order to implement effective boundary conditions (2.29) or (2.30), one needs to compute the quantity $\langle \beta_{\bar{\boldsymbol{x}}_P} \rangle$, i.e., a *parameter dependent* solution of the cell problem (2.23). The entailed frequent queries of the solutions to a *parameter dependent* family of cell problems can be facilitated at acceptable cost by employing reduced basis methods for the arising convection-diffusion equations, see e.g. [15]. Since this is beyond the scope of the current paper we will address this in future work. In the present article we will simply approximate $\langle \beta_{\bar{\boldsymbol{x}}_P} \rangle$ by a piecewise linear function $\langle \beta_{\bar{\boldsymbol{x}}_P} \rangle^*$, obtained solving the cell problem at certain locations $\bar{\boldsymbol{x}}_P^{(i)}$, $i=1,...,N$, $\bar{\boldsymbol{x}}_P^{(i)} \in \Gamma_0$.

3 Application: Laminar fluid flow over a rough wall

We now apply the strategy presented in Section 2 to steady, laminar, subsonic flow of a perfect gas over a wall with embedded periodic roughness. We formulate first the exact problem and the corresponding zeroth order problem, to derive then the cell problem and the effective problem. In particular, we will address the special features that arise for a system of equations.

3.1 The exact problem: Mathematical model

As in [16, 17], the flow field in the rough domain Ω^ϵ is modeled by the steady compressible Navier-Stokes equations (NSE) composed of the balance laws for mass, momentum and total energy. Denoting by Re the Reynolds number they read in dimensionless form as

$$\begin{aligned} \nabla \cdot (\rho \boldsymbol{u}) &= 0, \\ \nabla \cdot (\rho \boldsymbol{u} \otimes \boldsymbol{u}) + \nabla p &= \tfrac{1}{Re} \nabla \cdot \sigma, \\ \nabla \cdot ((\rho E + p) \boldsymbol{u}) &= \tfrac{1}{Re} \nabla \cdot (\sigma \boldsymbol{u} - \boldsymbol{q}), \end{aligned} \tag{3.1}$$

for the conserved quantities $(\rho, \rho \boldsymbol{u}, \rho E)$ with density ρ, velocity $\boldsymbol{u} = (u_1,...,u_d)^T$, pressure p and total energy $E = e + \tfrac{1}{2} \boldsymbol{u}^2$ composed of internal energy e and kinetic energy. Denoting by $\mathbb{I}$ the identity matrix, the viscous stress tensor σ and the heat flux $\boldsymbol{q}$ for an isentropic Newtonian fluid are defined by

$$\sigma \equiv \sigma(\boldsymbol{u}) = -\frac{2}{3} \eta (\nabla \cdot \boldsymbol{u}) \mathbb{I} + \eta (\nabla \boldsymbol{u} + (\nabla \boldsymbol{u})^T), \quad \boldsymbol{q} \equiv \boldsymbol{q}(T) = -\frac{\gamma}{Pr} \kappa \nabla T, \tag{3.2}$$

where we have used Fourier's law and Pr is the Prandtl number. Here η and κ denote the dynamic shear viscosity coefficient and the heat conductivity coefficient, respectively, both assumed to be constant, and T the temperature. The system (3.1) is closed by the calorical and thermal equations of state for a perfect gas

$$e = T, \quad p = \rho e (\gamma - 1) = \rho R T, \tag{3.3}$$

with γ the ratio of specific heats at constant pressure and volume, respectively. Furthermore, we introduce the mass specific enthalpy h and the sound speed c. For a perfect gas these are determined by

$$h = e + p/\rho = \frac{p}{\rho}\frac{\gamma}{\gamma-1}, \quad c^2 = \gamma p/\rho = \gamma RT. \tag{3.4}$$

Note that throughout this work we will use dimensionless quantities.

In the following we will always assume that the following assumptions hold.

Hypothesis: 3.1.

(i) The flow is subsonic, i.e., the Mach number $M = |\boldsymbol{u}|/c$ is less than one in the flow field.

(ii) The flow is laminar, i.e., the Reynolds number is in the range of 1×10^3 to 5×10^5.

Since the flow is subsonic, no shocks develop due to compressibility effects and the solution of the problem is smooth. In particular, it allows us to consider the system (3.1) written in *conservative form*, in the equivalent *quasi-conservative form* for the primitive variables $u := (\rho, \boldsymbol{u}, p)$, i.e., (3.1) becomes

$$\mathcal{L}(u) := \begin{pmatrix} (\boldsymbol{u}\cdot\nabla)\rho + \rho\nabla\cdot\boldsymbol{u} \\ (\boldsymbol{u}\cdot\nabla)\boldsymbol{u} + \frac{1}{\rho}\nabla p - \frac{1}{\rho Re}\nabla\cdot\sigma \\ (\boldsymbol{u}\cdot\nabla)p + \gamma p(\nabla\cdot\boldsymbol{u}) + \frac{\gamma-1}{Re}((\sigma\cdot\nabla)\cdot\boldsymbol{u} + \nabla\cdot\boldsymbol{q}) \end{pmatrix} = 0, \tag{3.5}$$

where we have employed the equation of state (3.3). Thus the solution $u^\epsilon = (\rho^\epsilon, \boldsymbol{u}^\epsilon, p^\epsilon)$ in the rough domain Ω^ϵ satisfies

$$\mathcal{L}(u^\epsilon) = 0 \quad \text{in} \quad \Omega^\epsilon. \tag{3.6}$$

In view of Hypothesis 3.1, we impose at the various boundary portions of Ω^ϵ, see Figure 3, subsonic free-stream conditions ρ_∞, p_∞, $\boldsymbol{u}_\infty = u_\infty \boldsymbol{e}_1$ with $M_\infty < 1$ at the inflow boundary Γ_{in}, far-field conditions at the upper boundary Γ_{far}, subsonic outflow conditions characterized by the pressure p_{out} at Γ_{out} and slip conditions at Γ_{sp}. At the rough wall Γ_ϵ we impose no-slip conditions where the wall is either adiabatic or isothermal:

$$\rho^\epsilon = \rho_\infty, \qquad \frac{\partial p^\epsilon}{\partial n} = 0, \quad \boldsymbol{u}^\epsilon = \boldsymbol{u}_\infty \qquad\qquad\qquad \text{on} \quad \Gamma_{in}, \tag{3.7a}$$

$$\frac{\partial \rho^\epsilon}{\partial n} = 0, \qquad p^\epsilon = p_\infty, \quad \boldsymbol{u}^\epsilon = \boldsymbol{u}_\infty \qquad\qquad\qquad \text{on} \quad \Gamma_{far}, \tag{3.7b}$$

$$\frac{\partial \rho^\epsilon}{\partial n} = 0, \qquad p^\epsilon = p_{out}, \quad \frac{\partial \boldsymbol{u}^\epsilon}{\partial n} = 0 \qquad\qquad\qquad \text{on} \quad \Gamma_{out}, \tag{3.7c}$$

$$\rho^\epsilon = \rho_\infty, \qquad p^\epsilon = p_\infty, \quad u_1^\epsilon = u_\infty, \quad \frac{\partial u_{2,3}^\epsilon}{\partial n} = 0 \qquad \text{on} \quad \Gamma_{sp}, \tag{3.7d}$$

$$\frac{\partial \rho^\epsilon}{\partial n} = 0, \qquad \frac{\partial p^\epsilon}{\partial n} = 0, \quad \boldsymbol{u}^\epsilon = \boldsymbol{0} \qquad\qquad \text{on} \quad \Gamma_\epsilon \text{ (adiabatic) or} \tag{3.7e}$$

$$\rho^\epsilon = \rho_{wall}, \qquad \frac{\partial p^\epsilon}{\partial n} = 0, \quad \boldsymbol{u}^\epsilon = \boldsymbol{0} \qquad\qquad \text{on} \quad \Gamma_\epsilon \text{ (isothermal).} \tag{3.7f}$$
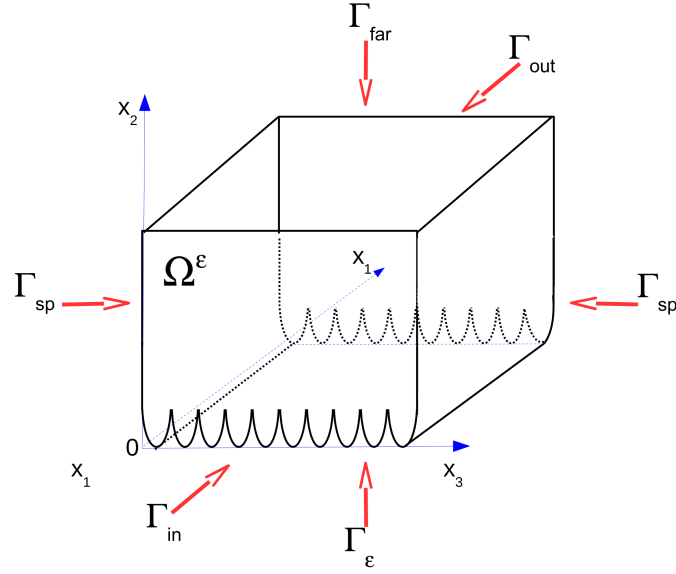
Figure 3: Boundaries on macro-scale domain Ω^ϵ.

Since the conditions (3.7a), (3.7b) and (3.7c) on the inflow, far field, outflow and slip boundary, respectively, will not be affected by the zeroth order problem and the effective problem, we summarize for convenience these boundary conditions for the respective boundary portions as

$$\bar{\mathcal{B}}_{in}(u^\epsilon)=0, \quad \bar{\mathcal{B}}_{far}(u^\epsilon)=0, \quad \bar{\mathcal{B}}_{out}(u^\epsilon)=0, \quad \bar{\mathcal{B}}_{sp}(u^\epsilon)=0. \tag{3.8}$$

These correspond to the operator $\bar{\mathcal{B}}$ in (2.1c). Accordingly, at Γ_ϵ the adiabatic or isothermal boundary conditions read

$$\mathcal{B}_{adiabatic}(u^\epsilon)=0, \quad \mathcal{B}_{isothermal}(u^\epsilon)=0. \tag{3.9}$$

Finally, the exact problem (2.1) is determined by (3.6), (3.7), and (3.8), (3.9), respectively.

3.2 Zeroth order approximation

According to (2.8) the zeroth order solution has to be the solution of the Navier-Stokes equations on the smooth domain Ω^0, i.e., the solution $u^0=(\rho^0,\boldsymbol{u}^0,p^0)$ satisfies

$$\mathcal{L}(u^0)=0 \quad \text{in} \quad \Omega^0 \tag{3.10}$$

with boundary conditions

$$\bar{\mathcal{B}}_{in}(u^0)=0, \quad \bar{\mathcal{B}}_{far}(u^0)=0, \quad \bar{\mathcal{B}}_{out}(u^0)=0, \quad \bar{\mathcal{B}}_{sp}(u^0)=0, \tag{3.11a}$$

$$\frac{\partial \rho^0}{\partial n}=0, \qquad\qquad \frac{\partial p^0}{\partial n}=0, \quad u^0=\mathbf{0} \qquad\qquad \text{on} \quad \Gamma_0 \text{ (adiabatic) or} \tag{3.11b}$$

$$\rho^0=\rho_{wall}, \qquad\quad \frac{\partial p^0}{\partial n}=0, \quad u^0=\mathbf{0} \qquad\qquad \text{on} \quad \Gamma_0 \text{ (isothermal).} \tag{3.11c}$$
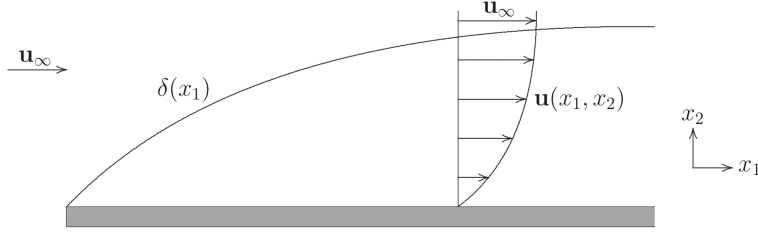
Figure 4: Sketch of the zeroth order solution for a fixed x_3.

The zeroth order problem thus corresponds to the flow over a flat plate. Due to Hypothesis 3.1 the solution is determined by a laminar boundary layer sketched in Figure 4, where the boundary layer thickness can be approximated by $\delta \sim 4.91 x / \sqrt{Re_x}$, cf. [46]. A good approximation is given by van Driest's similarity solution [5]. As a consequence of this choice, the pressure p^0 is constant in the whole domain, i.e.,

$$p^0 = p_\infty = const \tag{3.12}$$

and there is no flow in wall-normal direction or spanwise direction ($d=3$), i.e.,

$$u^0(x) = (u_1^0(x),0,0)^T, \quad \frac{\partial u_i^0}{\partial x_2}(x)=0, \, i=2,...,d, \, x\in\Omega^0 , \tag{3.13}$$

and $\partial\rho^0(x)/\partial x_3 = 0$, $x\in\Omega^0$. Moreover, in the isothermal case ρ_{wall} is constant at Γ_0, i.e., $\partial\rho^0(x)/\partial x_i=0$, $x\in\Gamma_0$, $i\neq 2$.

Note that when restricting u^0 to a given roughness element $R(\bar{x}_P)$ its variation in streamwise direction within this element is negligible. As an input in the corresponding cell problems u^0 will always be understood to be the piecewise constant in streamwise direction defined by

$$u_j^0(\mathcal{Y}_{\bar{x}_P}^{-1}(y))=0, \quad y\in Y, j\neq 1, \quad \begin{cases} u_1^0(x)=u_1^0(\mathcal{Y}_{\bar{x}_P}^{-1}(0,y_2,0))\neq 0, \\ \rho^0(x)=\rho^0(\mathcal{Y}_{\bar{x}_P}^{-1}(0,y_2,0)), \\ p^0(x)=p^0(\mathcal{Y}_{\bar{x}_P}^{-1}(0,y_2,0)), \end{cases} , x\in R(\bar{x}_P) . \tag{3.14}$$

3.3 Cell problem

In order to determine the cell problem (2.23) for the above system we first define for each quantity the upscaling functions $u^1=(\rho^1,u^1,p^1)$ and corresponding rescaled cell function $\beta=(\phi,\chi,\pi)$,

according to (2.41). To distinguish derivatives with respect to x and y we use ∇, Δ and ∇_y, Δ_y, respectively.

To each equation in (3.5) we apply the strategy described in Section 2. Doing so (2.13) is given by

$$\mathcal{C}_{\bar{x}_P}((\phi,\chi,\pi))(y)=0, \quad y\in Y, \tag{3.15}$$

where $\mathcal{C}=(\mathcal{C}_\phi,\mathcal{C}_\chi,\mathcal{C}_\pi)^T$, i.e., each component of $\mathcal{C}$ corresponds to the continuity, the velocity and the pressure equation, respectively. A componentwise application of the strategy described in **Step 3a** of the previous section (see also the examples there), one obtains

$$
\begin{aligned}
\mathcal{C}_\phi &:= (u^0\cdot\nabla_y)\phi+\rho^0\nabla_y\cdot\chi\,,\\
\mathcal{C}_\chi &:= \rho^0(u^0\cdot\nabla_y)\chi+\nabla_y\pi-\tfrac{\eta}{\epsilon Re}\left(\Delta_y\chi+\tfrac{1}{3}\nabla_y(\nabla_y\cdot\chi)\right),\\
\mathcal{C}_\pi &:= (u^0\cdot\nabla_y)\pi+\gamma p^0\nabla_y\cdot\chi-\tfrac{1}{\epsilon Re}\tfrac{\gamma\kappa}{Pr\rho^0}\left(\Delta_y\pi-\tfrac{p^0}{\rho^0}\Delta_y\phi\right)+\tfrac{\eta}{Re}\mathcal{T}_{\bar{x}_P}(\chi)\,.
\end{aligned}
\tag{3.16}
$$

Note that the term $\mathcal{T}_{\bar{x}_P}(\chi)$ in (3.16) is nonlinear and has the form

$$\mathcal{T}_{\bar{x}_P}(\chi):=t_{xy}(u^0,\chi)+t_{yx}(\chi,u^0)+t_{yy}(\chi,\chi)\,, \tag{3.17}$$

with

$$t_{\zeta\xi}(\mathbf{z},\mathbf{w}):=\left(\left(-\frac{2}{3}(\nabla_\zeta\cdot\mathbf{z})\mathbb{I}+\nabla_\zeta\mathbf{z}+(\nabla_\zeta\mathbf{z})^T\right)\cdot\nabla_\xi\right)\cdot\mathbf{w}\,.$$

Thus the cell problem (3.15) is a nonlinear system. However, under the following assumption, $\mathcal{C}$ can be significantly simplified.

Roughness Scale: 3.1. Given the Reynolds number Re, we consider the range $\epsilon=\mathcal{O}(Re^{-\alpha})$, for some $\alpha>0$.

Observe that for this range of ϵ the cell operators $\mathcal{C}_\pi$ involves coefficients of orders $\mathcal{O}(1)$, $\mathcal{O}(Re^{\alpha-1})$ and $\mathcal{O}(Re^{-1})$. Specifically, $\frac{\eta}{Re}\mathcal{T}$ and $\frac{1}{\epsilon Re}\frac{\gamma\kappa}{Pr\rho^0}\left(\Delta_y\pi-\frac{p^0}{\rho^0}\Delta_y\phi\right)$ are of order $\mathcal{O}(Re^{-1})$ and $\mathcal{O}(Re^{\alpha-1})$, respectively. Since in the range of Hypothesis 3.1, Re is between $\mathcal{O}(10^3)$ and $\mathcal{O}(10^5)$, it follows that $\frac{\eta}{Re}\mathcal{T}$ is negligible in comparison to the other terms. Moreover, when ϵ is chosen smaller and smaller relative to Re^{-1}, i.e., when α is increased, the viscous term $\frac{1}{\epsilon Re}\frac{\gamma\kappa}{Pr\rho^0}\left(\Delta_y\pi-\frac{p^0}{\rho^0}\Delta_y\phi\right)$ dominates all other terms. Conversely, when α tends to 0^+, i.e., for increasing ϵ, the convective part $(u^0\cdot\nabla_y)\pi+\gamma p^0\nabla_y\cdot\chi$ dominates all other terms.

Thus, the Roughness Scale 3.1 justifies neglecting the term $\frac{\eta}{Re}\mathcal{T}$. As a consequence the cell problem $\mathcal{C}=0$ becomes linear.

Since in (3.7e) and (3.7f) Dirichlet boundary conditions are applied to the velocity u^ϵ and homogeneous Neumann conditions for the pressure p^ϵ, respectively, the following boundary conditions are imposed on W: (2.20) gives

$$\mathcal{C}_{Dir,\chi}(y) := \chi(y)+y_j\frac{\partial u^0}{\partial x_j}(\bar{x}_P)=0 \tag{3.18}$$

while (2.21) yields

$$C_{Neu,\pi}(\boldsymbol{y}) \quad := \quad \frac{\partial \pi}{\partial n_y^\epsilon}(\boldsymbol{y}). \tag{3.19}$$

Furthermore, in the adiabatic case (3.7e), homogeneous Neumann boundary conditions are imposed also on the density resulting in

$$C_{Neu,\phi}(\boldsymbol{y}) \quad := \quad \frac{\partial \phi}{\partial n_y^\epsilon}(\boldsymbol{y}), \tag{3.20}$$

whereas in the isothermal case (3.7f) we obtain

$$C_{Dir,\phi}(\boldsymbol{y}) \quad := \quad \phi(\boldsymbol{y}) + y_j \frac{\partial \rho^0}{\partial x_j}(\bar{\boldsymbol{x}}_P) = 0 \,. \tag{3.21}$$

Hence for our particular choice of the zeroth order problem, the boundary conditions (3.18), (3.19), (3.20) and (3.21) of the cell problems on W read now

$$\frac{\partial \pi}{\partial n_y^\epsilon}(\boldsymbol{y}) = 0, \quad \frac{\partial \phi}{\partial n_y^\epsilon}(\boldsymbol{y}) = 0, \quad \chi(\boldsymbol{y}) = -y_2 \frac{\partial u_1^0}{\partial x_2}(\bar{\boldsymbol{x}}_P)\boldsymbol{e}_1 \,, \tag{3.22}$$

in the adiabatic case, and

$$\frac{\partial \pi}{\partial n_y^\epsilon}(\boldsymbol{y}) = 0, \quad \phi(\boldsymbol{y}) = -y_2 \frac{\partial \rho^0}{\partial x_2}(\bar{\boldsymbol{x}}_P), \quad \chi(\boldsymbol{y}) = -y_2 \frac{\partial u_1^0}{\partial x_2}(\bar{\boldsymbol{x}}_P)\boldsymbol{e}_1 \,, \tag{3.23}$$

in the isothermal one.

We conclude the section proving the validity of part (II) of Hypothesis 2.1 in the present setting.

Theorem 3.1. *Assume that the zeroth order solution $\boldsymbol{u}^0$ of (3.10) satisfies (3.14). If the cell function β satisfies the conditions in Hypothesis 2.1, then for every $1 \le y_2$ one has*

$$\frac{\partial}{\partial y_2} \int_{\Gamma_{up}^{y_2}} \beta d\gamma = 0, \quad y_2 \ge 1, \quad \beta \in \{\pi, \phi, \chi\}, \tag{3.24}$$

where $\Gamma_{up}^{\bar{y}_2} := \{\boldsymbol{y} \in Y : y_2 = \bar{y}_2\}$, for some $\bar{y}_2 \ge 1$.

For simplicity we prove the Theorem for $d = 2$ building essentially on the ideas in [32]. The proof can be easily extended for $d > 2$. First we can reexpress (3.24) by requiring that for each $1 \le a < b$

$$\begin{aligned}
\int_{-s}^s \pi(y_1, a) dy_1 &= \int_{-s}^s \pi(y_1, b) dy_1 \,, \\
\int_{-s}^s \phi(y_1, a) dy_1 &= \int_{-s}^s \phi(y_1, b) dy_1 \,, \\
\int_{-s}^s \chi_k(y_1, a) dy_1 &= \int_{-s}^s \chi_k(y_1, b) dy_1 \,, \ k = 1, 2 \,.
\end{aligned} \tag{3.25}$$

Integrating the first equation of (3.15) at $y_2 = b$ and using the periodicity of ϕ and χ_1 and $u_1^0(x) = u_1^0(x_2)$, we obtain

$$0 = \int_{-s}^{s} \frac{\partial \chi_1}{\partial y_1}(y_1, b) dy_1 = -\int_{-s}^{s} \frac{\partial \chi_2}{\partial y_2}(y_1, b) dy_1 \,, \tag{3.26}$$

for each $b \geq 1$. Next, integrating the second equation of (3.15) over the volume $V := (-s, s) \times (a, b)$ and using the periodicity of ϕ and χ as well as the fact that $u_1^0(x) = u_1^0(x_2)$, $\rho^0(x) = \rho^0(x_2)$, the divergence theorem yields

$$
\begin{aligned}
\mathbf{0} &= \int_V \frac{\eta}{\epsilon Re} \Delta \chi - \nabla \pi \, dv = \int_{\partial V} \left(\frac{\eta}{\epsilon Re} \nabla \chi - \pi \mathbb{I} \right) \cdot \mathbf{n} d\sigma \\
&= \begin{pmatrix} \int_{-s}^{s} \frac{\eta}{\epsilon Re} \left(\frac{\partial \chi_1}{\partial y_2}(y_1, b) - \frac{\partial \chi_1}{\partial y_2}(y_1, a) \right) dy_1 \\ \int_{-s}^{s} \frac{\eta}{\epsilon Re} \left(\frac{\partial \chi_2}{\partial y_2}(y_1, b) - \frac{\partial \chi_2}{\partial y_2}(y_1, a) \right) - \pi(y_1, b) + \pi(y_1, a) dy_1 \end{pmatrix} .
\end{aligned}
\tag{3.27}
$$

Using the second relation in (3.26) for $a, b \geq 1$, we infer from the second component of the right-hand side of (3.27) that

$$\int_{-s}^{s} \pi(y_1, a) dy_1 = \int_{-s}^{s} \pi(y_1, b) dy_1, \quad a < b, \tag{3.28}$$

which is the first relation in (3.25) and, under the given assumptions, means

$$\frac{\partial}{\partial y_2} \int_{-s}^{s} \pi(y_1, b) dy_1 = \int_{-s}^{s} \frac{\partial \pi}{\partial y_2}(y_1, b) dy_1 = 0, \quad b \geq 1. \tag{3.29}$$

Now we multiply the third equation of (3.15) by $y_2 - a$, integrate over V and apply the divergence theorem. Using the periodicity of ϕ and π and $u_1^0(x) = u_1^0(x_2)$, $\rho^0(x) = \rho^0(x_2)$, $p^0(x) = p^0(x_2)$, one eventually obtains

$$\int_{-s}^{s} (b-a) \frac{\partial}{\partial y_2} \phi(y_1, b) dy_1 + \int_{-s}^{s} \phi(y_1, a) - \phi(y_1, b) dy_1 = 0.$$

Fixing a and taking b sufficiently large, we infer from Hypothesis 2.1 (I) that $\left| \int_{-s}^{s} \phi(y_1, a) - \phi(y_1, b) dy_1 \right|$ is arbitrarily small. Since this is true for each a we conclude that

$$\int_{-s}^{s} \phi(y_1, a) dy_1 = \int_{-s}^{s} \phi(y_1, b) dy_1,$$

which is the second equation in (3.25).

To verify the remaining claim we proceed similarly, multiplying the second equation of (3.15) by $b - y_2$ and integrating it over V. Once more we use the periodicity of ϕ and χ and $u_1^0(x) = u_1^0(x_2)$, $\rho^0(x) = \rho^0(x_2)$, and apply the divergence theorem to obtain

$$
\begin{pmatrix} \int_{-s}^{s} \frac{\eta}{\epsilon Re} (\chi_1(y_1, b) - \chi_1(y_1, a)) dy_1 \\ \int_{-s}^{s} \frac{\eta}{\epsilon Re} (\chi_2(y_1, b) - \chi_2(y_1, a)) dy_1 - \int_V \pi dv \end{pmatrix} =
\tag{3.30}
$$
$$
\begin{pmatrix} \int_{-s}^{s} (b-a) \frac{\eta}{\epsilon Re} \frac{\partial \chi_1}{\partial y_2}(y_1, a) dy_1 \\ \int_{-s}^{s} (b-a) \left(\frac{\eta}{\epsilon Re} \frac{\partial \chi_2}{\partial y_2}(y_1, a) - \pi(y_1, a) \right) dy_1 \end{pmatrix} .
$$

From (3.29) we infer next that for any $1 \leq a \leq b$

$$\int_V \pi d\mathbf{y} = \int_a^b \left(\int_{-s}^s \pi(y_1, y_2) dy_1 \right) dy_2 = (b-a) \int_{-s}^s \pi(y_1, a) dy_1 .$$

Thus the last terms in the second component on both sides of (3.30), respectively, are equal and hence can be dropped. Moreover, we deduce from the first component of the right-hand side of (3.27) that

$$\int_{-s}^s \frac{\partial \chi_1}{\partial y_2}(y_1, a) dy_1 = \int_{-s}^s \frac{\partial \chi_1}{\partial y_2}(y_1, b) dy_1, \quad a < b,$$

which means that $\int_{-s}^s \chi_1(y_1, y_2) dy_1$ has a constant slope as a function of y_2. By part (I) in Hypothesis 2.1 this slope must be zero. Thus $\int_{-s}^s \frac{\partial \chi_1}{\partial y_2}(y_1, a) dy_1 = 0$, which, again by the first line of (3.30), implies

$$\int_{-s}^s \frac{\eta}{\epsilon Re}(\chi_1(y_1, b) - \chi_1(y_1, a)) dy_1$$

which is the case $k = 1$ in the third line of (3.25). On the other hand, by (3.26), $\int_{-s}^s \frac{\partial \chi_2}{\partial y_2}(y_1, y_2) dy_1 = 0$ for each $y_2 \geq 1$, which also shows that $\int_{-s}^s \chi_2(y_1, a) dy_1 = \int_{-s}^s \chi_2(y_1, b) dy_1$, for $1 \leq a \leq b$, and finishes the proof. $\qquad \square$

The above argument shows that the conditions in Hypothesis 2.1 (I) are only needed for the quantities ϕ, χ_1.

3.4 Effective problem

According to (2.6), the effective problem then reads

$$\mathcal{L}(u^{eff}) = 0 \quad \text{in} \quad \Omega^\sigma \tag{3.31}$$

with boundary conditions

$$\bar{\mathcal{B}}_{in}(u^{eff}) = 0, \quad \bar{\mathcal{B}}_{far}(u^{eff}) = 0, \quad \bar{\mathcal{B}}_{out}(u^{eff}) = 0, \quad \bar{\mathcal{B}}_{sp}(u^{eff}) = 0 . \tag{3.32}$$

Specifically, the *implicit* version of boundary conditions reads now

$$\frac{\partial p^{eff}}{\partial x_2}(\mathbf{x}) = 0, \quad u^{eff}(\mathbf{x}) - \sigma \frac{\partial u_1^{eff}}{\partial x_2}(\mathbf{x}) e_1 = \epsilon \langle \chi \rangle, \quad \text{on} \quad \Gamma_\sigma \cap R(\bar{x}_P) \tag{3.33a}$$

$$\frac{\partial \rho^{eff}}{\partial x_2}(\mathbf{x}) = \sigma \frac{\partial^2 \rho^{eff}}{\partial x_2^2}(\mathbf{x}) \quad \text{(adiabatic) or} \tag{3.33b}$$

$$\rho^{eff}(\mathbf{x}) - \sigma \frac{\partial \rho^{eff}}{\partial x_2}(\mathbf{x}) = \rho_{wall} + \epsilon \langle \phi \rangle, \quad \mathbf{x} \in \Gamma_\sigma \cap R(\bar{x}_P) \quad \text{(isothermal)}. \tag{3.33c}$$

As *explicit boundary conditions* we have now

$$\frac{\partial p^{eff}}{\partial x_2}(\boldsymbol{x}) = 0, \quad \boldsymbol{u}^{eff}(\boldsymbol{x}) = \boldsymbol{u}^0(\boldsymbol{x}) + \epsilon \langle \boldsymbol{\chi} \rangle, \quad \boldsymbol{x} \in \Gamma_\sigma \cap R(\bar{\boldsymbol{x}}_P) \tag{3.34a}$$

$$\frac{\partial \rho^{eff}}{\partial x_2}(\boldsymbol{x}) = \frac{\partial \rho^0}{\partial x_2}(\boldsymbol{x}) \quad \text{(adiabatic) or} \tag{3.34b}$$

$$\rho^{eff}(\boldsymbol{x}) = \rho^0(\boldsymbol{x}) + \epsilon \langle \phi \rangle, \quad \boldsymbol{x} \in \Gamma_\sigma \cap R(\bar{\boldsymbol{x}}_P) \quad \text{(isothermal).} \tag{3.34c}$$

These effective boundary conditions are derived according to Step 4 of Section 2, where, depending on the boundary conditions applied to each variable u_i^0, ρ^0 and p^0, we use either (2.29) or (2.30) in the Dirichlet and either (2.35) or (2.36) in the Neumann case with

$$
\begin{aligned}
\mathcal{J}_{D,u_i^0} &= \left\{ j \in \{1,...,d\}, \, s.t. \, \partial u_i^0 / \partial x_j(\bar{\boldsymbol{x}}_P) \neq 0 \right\} = \begin{cases} \{2\}, \, i = 1 \\ \varnothing, \, i \neq 1 \end{cases}, \\
\mathcal{J}_{D,\rho^0} &= \left\{ j \in \{1,...,d\}, \, s.t. \, \partial \rho^0 / \partial x_j(\bar{\boldsymbol{x}}_P) \neq 0 \right\} = \{2\}, \, \text{(isothermal)} , \\
\mathcal{J}_{N,p^0} &= \left\{ j \in \{1,...,d\}, \, s.t. \, \partial^2 p^0 / \partial x_2 \partial x_j(\bar{\boldsymbol{x}}_P) \neq 0 \right\} = \varnothing , \\
\mathcal{J}_{N,\rho^0} &= \left\{ j \in \{1,...,d\}, \, s.t. \, \partial^2 \rho^0 / \partial x_2 \partial x_j(\bar{\boldsymbol{x}}_P) \neq 0 \right\} = \{2\}, \, \text{(adiabatic)} .
\end{aligned}
$$

4 Numerical Results

For an application we consider a laminar, subsonic flow over a rough surface, where the roughness is assumed to be periodic but anisotropic, i.e., longitudinal riblets, or isotropic, i.e. bumps. For an illustration of the different roughness elements see Figure 5. The exact and the smooth effective domains Ω^σ are sketched in Figure 6.

The flow field corresponds to the Reynolds number $Re_\infty = 10^5$. In the viscous stress tensor and the heat flux, see equation (3.2), the dynamic viscosity coefficient and the heat conductivity coefficient are chosen as $\eta = 1$ and $\kappa = 1$, respectively. The gas is assumed to be air, thus we use $Pr = 0.72$ for the Prandtl number and $\gamma = 1.4$ for the ratio of specific heats.

The free-stream conditions are determined by the free-stream Mach number $M_\infty = 0.3$ and $M_\infty = 0.6$, in the isothermal and the adiabatic case, respectively, and

$$\rho_\infty = 1, \, T_\infty = 1, \, \boldsymbol{u}_\infty = (1,0,0)^T, \, p_\infty = \frac{1}{M_\infty^2 \gamma}.$$

In the isothermal case we assume moreover that the temperature at the wall T_{wall} is equal to 0.586.

In **Appl.Sc.1** the zeroth order solution is approximated using the van Driest similarity solution, cf. [16]. In Figure 7 the flow quantities in wall-normal direction are depicted for different dimensionless positions on the flat plate in streamwise direction, cf. [16].

(a) Longitudinal riblets.

(b) Isotropic roughness.
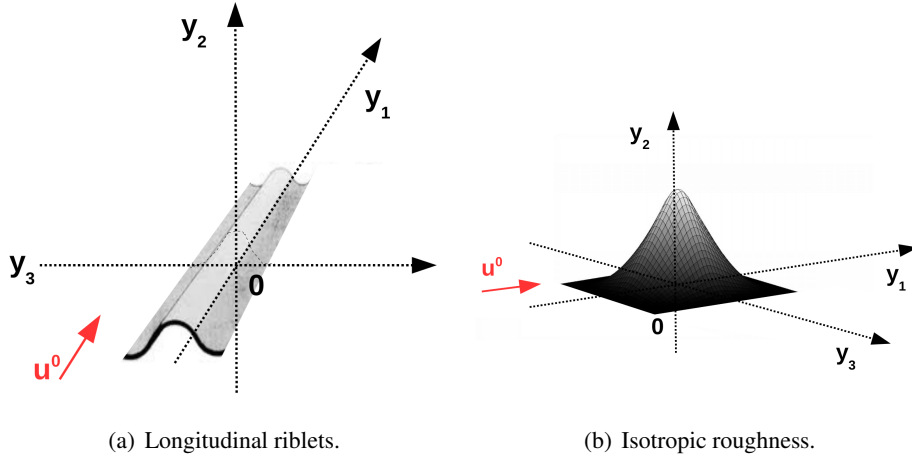
Figure 5: Sketch of cell domains.

(a) Exact domain.
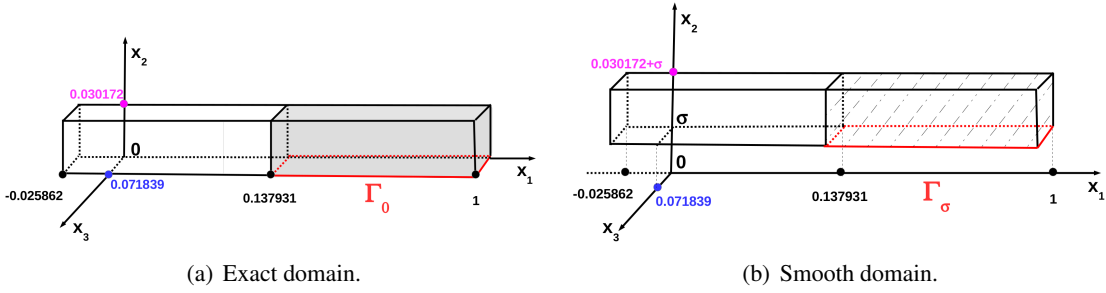
(b) Smooth domain.

Figure 6: Sketch of the smooth domains.

4.1 Cell Problem

The different roughness structures, cf. Figure 5, are determined by the C^1-curve introduced in [16] with $s = 10$, $r = 2\epsilon$, $R = 8\epsilon$ and $\epsilon = 5 \cdot 10^{-5} / L^*$ where $L^* = 0.0348$. More precisely, consider the function

$$f(\zeta) := \begin{cases} 1 - r/\epsilon + \sqrt{(r/\epsilon)^2 - (\zeta + 2s)^2}, & \text{if} \quad \zeta < -\hat{\zeta}_1, \\ \frac{\check{\zeta}_2 - \hat{\zeta}_2}{-\check{\zeta}_1 + \hat{\zeta}_1}(\zeta + \hat{\zeta}_1) + \hat{\zeta}_2, & \text{if} \quad -\hat{\zeta}_1 < \zeta < -\check{\zeta}_1, \\ R/\epsilon - \sqrt{(R/\epsilon)^2 - \zeta^2}, & \text{if} \quad -\check{\zeta}_1 < \zeta < \check{\zeta}_1, \\ \frac{\check{\zeta}_2 - \hat{\zeta}_2}{\check{\zeta}_1 - \hat{\zeta}_1}(\zeta - \hat{\zeta}_1) + \hat{\zeta}_2, & \text{if} \quad \check{\zeta}_1 < \zeta < \hat{\zeta}_1, \\ 1 - r/\epsilon + \sqrt{(r/\epsilon)^2 - (\zeta - 2s)^2}, & \text{if} \quad \zeta > \hat{\zeta}_1, \end{cases} \qquad (4.1)$$

(a) Adiabatic case. (b) Isothermal case.
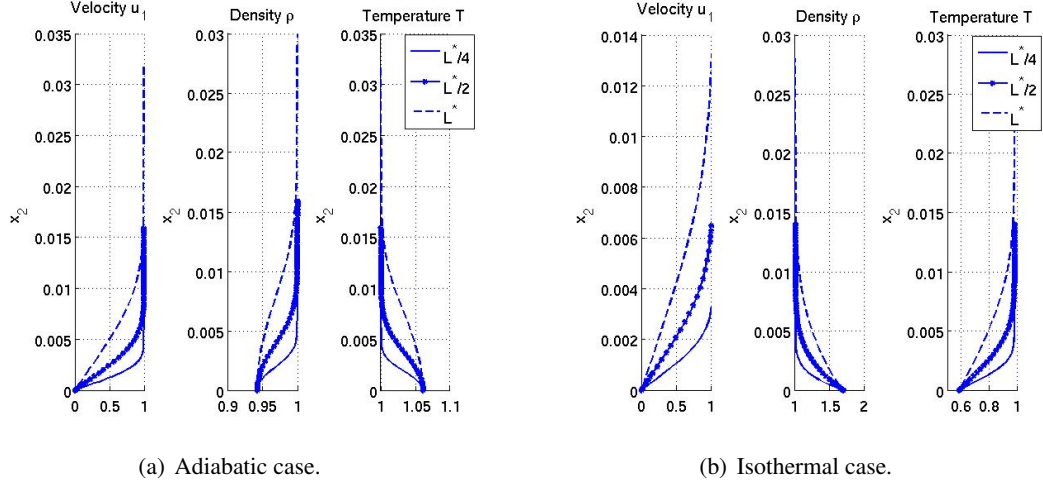
Figure 7: Boundary layer solution in wall-normal direction for several dimensionless positions in streamwise direction $\bar{\xi} = L^*/4, L^*/2, L^*$ on the flat plate: streamwise velocity u_1 (left), density ρ (middle), temperature T (right).

with $(\check{\zeta}_1, \check{\zeta}_2) = (2.1098, 0.28321)$ and $(\hat{\zeta}_1, \hat{\zeta}_2) = (4.4726, 0.9292)$. Then for longitudinal riblets and isotropic roughness one has

$$
\begin{aligned}
W_{rib} &= \left\{ (y_1, y_2, y_3), \text{ s.t. } y_1 \in [-s/2, s/2], \, y_2 = f(y_3), \, y_3 \in [-s/2, s/2] \right\}, \\
W_{bump} &= \left\{ (y_1, y_2, y_3), \text{ s.t. } y_1 \in [-s/2, s/2], \, y_2 = f(y_1)f(y_3), \, y_3 \in [-s/2, s/2] \right\},
\end{aligned}
$$

respectively. Moreover to bound Y we choose

$$
\begin{aligned}
\Gamma_{up,rib} &= \left\{ (y_1, y_2, y_3), \text{ s.t. } y_1 \in [-s/2, s/2], \, y_2 = 10, \, y_3 \in [-s/2, s/2] \right\}, \\
\Gamma_{up,bump} &= \left\{ (y_1, y_2, y_3), \text{ s.t. } y_1 \in [-s/2, s/2], \, y_2 = 7, \, y_3 \in [-s/2, s/2] \right\}.
\end{aligned}
$$

Then, according to Hypothesis 3.1, for each configuration we solve one cell problem at different positions $\bar{x}_P$, i.e.,

$$
\begin{aligned}
(\boldsymbol{u}^0 \cdot \nabla_y)\phi + \rho^0 \nabla_y \cdot \boldsymbol{\chi} &= 0, \\
\rho^0 (\boldsymbol{u}^0 \cdot \nabla_y)\boldsymbol{\chi} + \nabla_y \pi &= \frac{\eta}{\epsilon Re} \left(\Delta_y \boldsymbol{\chi} + \tfrac{1}{3} \nabla_y (\nabla_y \cdot \boldsymbol{\chi}) \right), \\
(\boldsymbol{u}^0 \cdot \nabla_y)\pi + \gamma p^0 \nabla_y \cdot \boldsymbol{\chi} &= \frac{1}{\epsilon Re} \frac{\gamma \kappa}{Pr \rho^0} \left(\Delta_y \pi - \frac{p^0}{\rho^0} \Delta_y \phi \right),
\end{aligned}
\tag{4.2}
$$

with boundary conditions on W

$$
\begin{aligned}
\boldsymbol{\chi}(\boldsymbol{y}) &= -y_2 \frac{\partial u_1^0}{\partial x_2}(\bar{x}_P)\boldsymbol{e}_1, & \frac{\partial \pi}{\partial n_y^\epsilon}(\boldsymbol{y}) &= 0, & \frac{\partial \phi}{\partial n_y^\epsilon}(\boldsymbol{y}) &= 0, & \text{(adiabatic)} \\
\boldsymbol{\chi}(\boldsymbol{y}) &= -y_2 \frac{\partial u_1^0}{\partial x_2}(\bar{x}_P)\boldsymbol{e}_1, & \frac{\partial \pi}{\partial n_y^\epsilon}(\boldsymbol{y}) &= 0, & \phi(\boldsymbol{y}) &= -y_2 \frac{\partial \rho^0}{\partial x_2}(\bar{x}_P), & \text{(isothermal)}
\end{aligned}
\tag{4.3}
$$

and boundary conditions on Γ_{up}

$$\left(\tfrac{\eta}{\epsilon Re}\nabla\chi - \pi \mathbb{I}\right)n \;=\; 0, \quad \nabla\phi\cdot n \;=\; 0\,. \tag{4.4}$$

Moreover, we assume that χ, π and ϕ are periodic in y_1 and y_3.

Finally observe that in the adiabatic case ϕ is determined only up to a constant, thus, to have a unique solution, we need to impose an additional constraint, for example

$$\frac{1}{|Y|}\int_Y \phi = 0\,. \tag{4.5}$$

4.1.1   A specific feature of the cell problem

In this section we will show that, under the Hypothesis 2.1, our particular choice of the zeroth order solution, described in Section 3.2, entails that $\chi_2 = \chi_3 = 0$ in Y, i.e., only the first component χ_1 of the solution χ of the cell problem (4.2)-(4.4) is non-trivial. In particular, this holds true for both the isothermal and the adiabatic case, independent on the shape of the roughness. To see this we first infer from (4.3) that χ_2, χ_3 vanish on the boundary W, both in the adiabatic and the isothermal case. If we substitute now

$$\chi_2 = \chi_3 = 0, \quad \text{in } Y\,. \tag{4.6}$$

in (4.2), and take the properties of the zeroth order solution (3.13) and (3.14) into account, we obtain the following simplified system of equations:

$$u_1^0 \frac{\partial \phi}{\partial y_1} + \rho^0 \frac{\partial \chi_1}{\partial y_1} \;=\; 0\,, \tag{4.7}$$

$$\rho^0 u_1^0 \frac{\partial \chi_1}{\partial y_1} + \frac{\partial \pi}{\partial y_1} \;=\; \frac{\eta}{\epsilon Re}\left(\Delta_y \chi_1 + \frac{1}{3}\frac{\partial^2 \chi_1}{\partial y_1^2}\right)\,, \tag{4.8}$$

$$\frac{\partial \pi}{\partial y_2} \;=\; \frac{\eta}{\epsilon Re}\frac{1}{3}\frac{\partial^2 \chi_1}{\partial y_2 \partial y_1}\,, \tag{4.9}$$

$$\frac{\partial \pi}{\partial y_3} \;=\; \frac{\eta}{\epsilon Re}\frac{1}{3}\frac{\partial^2 \chi_1}{\partial y_3 \partial y_1}\,, \tag{4.10}$$

$$u_1^0 \frac{\partial \pi}{\partial y_1} + \gamma p^0 \frac{\partial \chi_1}{\partial y_1} \;=\; \frac{1}{\epsilon Re}\frac{\gamma\kappa}{Pr\rho^0}\left(\Delta_y \pi - \frac{p^0}{\rho^0}\Delta_y \phi\right)\,, \tag{4.11}$$

and (4.4) reads

$$\frac{\partial \chi_1}{\partial y_2} \;=\; 0, \quad \pi \;=\; 0, \quad \frac{\partial \phi}{\partial y_2} \;=\; 0, \quad \text{on } \Gamma_{up}\,. \tag{4.12}$$

Integrating then equations (4.9) and (4.10) with respect to y_2 and y_3, respectively, there exist suitable smooth functions $C_2(y_1,y_3)$ and $C_3(y_1,y_2)$ such that

$$\pi = \frac{\eta}{3\epsilon Re}\frac{\partial \chi_1}{\partial y_1} + C_2(y_1,y_3) = \frac{\eta}{3\epsilon Re}\frac{\partial \chi_1}{\partial y_1} + C_3(y_1,y_2)\,.$$

Then it follows that $C_2(y_1,y_3) = C_3(y_1,y_2) = C(y_1)$. Moreover, when y_2 tends to infinity, applying Hypothesis 2.1 we conclude that $\langle \pi \rangle = C(y_1)$, i.e. $C(y_1)$ is constant. Since on Γ_{up} π is zero, cf. (4.12), it follows that

$$\pi = \frac{\eta}{3\epsilon Re} \frac{\partial \chi_1}{\partial y_1} \,. \tag{4.13}$$

If we then substitute (4.13) in (4.8) and consider (4.3) and (4.12) we obtain that χ_1 must solve the problem

$$
\begin{aligned}
\rho^0 u_1^0 \frac{\partial \chi_1}{\partial y_1} &= \frac{\eta}{\epsilon Re} \Delta_y \chi_1 \,, & \text{in } Y \\
\chi_1(y) &= -y_2 \frac{\partial u_1^0}{\partial x_2}(\bar{x}_P) \,, & \text{on } W \\
\frac{\partial \chi_1}{\partial y_2} &= 0 \,, & \text{on } \Gamma_{up},
\end{aligned}
\tag{4.14}
$$

and is periodic in y_1 and y_3.

Consider now the following auxiliary variable $\alpha := -u_1^0 \phi - \rho^0 \chi_1$, which is obtained integrating (4.7) with respect to y_1. Note that u_1^0, ρ^0 and p^0 depend only on y_2, cf. Section 3.2. Using the fact that $u_1^0 \neq 0$ and substituting $\phi = -\frac{1}{u_1^0}\alpha - \frac{\rho^0}{u_1^0}\chi_1$, (4.14) and (4.13) in equation (4.11), we obtain the following problem for α:

$$
\begin{aligned}
\frac{1}{\epsilon Re}\frac{\gamma \kappa}{Pr} \Delta_y \alpha &= \frac{\eta(u_1^0 \rho^0)^2}{3\epsilon Re p^0}\frac{\partial^2 \chi_1}{\partial y_1^2} + \gamma u_1^0 (\rho^0)^2 \frac{\partial \chi_1}{\partial y_1} - \frac{\gamma\kappa (\rho^0)^2 u_1^0}{\epsilon Re Pr p^0}\left(\frac{1}{3}u_1^0 \frac{\partial^2 \chi_1}{\partial y_1^2} + p^0 \frac{\epsilon Re}{\eta}\frac{\partial \chi_1}{\partial y_1}\right) \,, & \text{in } Y \\
\frac{\partial}{\partial n_y^\epsilon}\left(\frac{\alpha}{u_1^0}\right) &= -\frac{\partial}{\partial n_y^\epsilon}\left(\frac{\rho^0}{u_1^0}\chi_1\right) & \text{(adiabatic)}, & \text{on } W \\
\alpha(y) &= y_2\left(\rho^0 \frac{\partial u_1^0}{\partial x_2}(\bar{x}_P) + u_1^0 \frac{\partial \rho^0}{\partial x_2}(\bar{x}_P)\right) & \text{(isothermal)}, & \text{on } W \\
\frac{\partial \alpha}{\partial y_2} &= 0 \,, & & \text{on } \Gamma_{up}.
\end{aligned}
\tag{4.15}
$$

Moreover, α is periodic in y_1 and y_3. Observe that in the adiabatic case we need an additional constraint. Since in (4.2) we impose (4.5), to be consistent we assume that α satisfies

$$\int_Y \frac{1}{u_1^0}\alpha = -\int_Y \frac{\rho^0}{u_1^0}\chi_1 \,. \tag{4.16}$$

To conclude, having successively solved (4.14) and (4.15), we compute from α and χ_1

$$\phi = -\frac{1}{u_1^0}\left(\rho^0 \chi_1 + \alpha\right) \,. \tag{4.17}$$

We can then state the following Proposition.

Proposition 4.1. Let the zeroth order solution (ρ^0, u^0, p^0) be chosen as described in Section 3.2 and satisfies (3.14). Moreover let ρ^0, u_1^0 and p^0 be bounded functions in each $R(\bar{x}_P)$ and let $u_1^0 \circ \mathcal{Y}_{\bar{x}_P}^{-1}$ be a monotonically increasing function in y_2. Then the following holds:

(I) There exists a unique weak solution $\bar{\chi}_1 \in H^1(Y)$ and $\bar{\alpha} \in H^1(Y)$ of (4.14) and (4.15), respectively, and thus $(\bar{\phi}, \bar{\chi}, \bar{\pi})$ with $\bar{\chi}_2$ and $\bar{\chi}_3$ satisfying (4.6) and $\bar{\phi} \in H^1(Y)$ and $\bar{\pi} \in L^2(Y)$ chosen according to (4.17) and (4.13), respectively, is uniquely determined.

(II) If $(\bar{\phi}, \bar{\chi}, \bar{\pi})$ is twice differentiable on Y, i.e., it is a strong solution of (4.17), (4.14), (4.6) and (4.13), then it is also a strong solution of (4.2) with boundary conditions (4.3) and (4.4).

(III) Given a strong solution $(\tilde{\phi}, \tilde{\chi}, \tilde{\pi})$ of the cell problem (4.2), (4.3), (4.4) satisfying Hypothesis 2.1, then $(\tilde{\phi}, \tilde{\chi}, \tilde{\pi})$ is a strong solution of (4.17), (4.14), (4.6) and (4.13).

The proof of (I) consists in applying the Lax Milgram theorem to the weak formulation of (4.14) and (4.15). (II) follows directly from plugging $(\bar{\phi}, \bar{\chi}, \bar{\pi})$ in (4.2),(4.3),(4.4). Finally (III) is proven in the way we construct $(\bar{\phi}, \bar{\chi}, \bar{\pi})$. $\qquad\square$

4.1.2 Longitudinal riblets

For longitudinal riblets the fully three-dimensional cell problem (4.2), (4.3), (4.4) can be reduced to two independent two-dimensional problems, defined in the two-dimensional domain depicted in Figure 8.
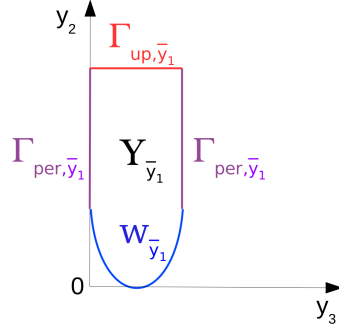
Figure 8: Longitudinal riblets: sketch of the domain $Y_{\bar{y}_1}$.

In fact if we deal with riblets aligned in streamwise direction x_1, the geometry is constant along y_1 in the cell domain. Moreover, using that u_0 varies only in wall normal direction, cf. (3.14), and that we impose periodic boundary conditions both in spanwise and in streamwise direction, all variables in the cell problem are constant in y_1. Thus the 3D cell problem (4.2) and (4.3) reduces to the following two two-dimensional problems defined in $(y_2, y_3) \in Y_{\bar{y}_1}$, i.e., $\bar{y}_1$-section of Y, sketched in Figure 8, cf. [25]:

$$
\begin{aligned}
\frac{\partial^2 \chi_1}{\partial y_2^2}(y) + \frac{\partial^2 \chi_1}{\partial y_3^2}(y) &= 0, \quad y \in Y_{\bar{y}_1}, \\
\chi_1(y) &= -\frac{\partial u_1^0}{\partial x_2}(\bar{x}_P) y_2, \quad y \in W_{\bar{y}_1}, \\
\nabla_y \chi_1(y) \cdot n(y) &= 0, \quad y \in \Gamma_{up, \bar{y}_1}, \\
y_3 &- \quad periodicity
\end{aligned}
\tag{4.18}
$$

and

$$\frac{\partial \chi_2}{\partial y_2}(y) + \frac{\partial \chi_3}{\partial y_3}(y) = 0, \quad y \in Y_{\bar{y}_1},$$

$$\frac{\partial^2 \pi}{\partial y_2^2}(y) = \frac{\eta}{\epsilon Re}\left(\frac{\partial^2 \chi_2}{\partial y_2^2}(y) + \frac{\partial^2 \chi_2}{\partial y_3^2}(y)\right),$$

$$\frac{\partial^2 \pi}{\partial y_3^2}(y) = \frac{\eta}{\epsilon Re}\left(\frac{\partial^2 \chi_3}{\partial y_2^2}(y) + \frac{\partial^2 \chi_3}{\partial y_3^2}(y)\right),$$

$$\frac{\partial^2 \pi}{\partial y_2^2}(y) + \frac{\partial^2 \pi}{\partial y_3^2}(y) = \frac{p^0}{\rho^0}\left(\frac{\partial^2 \phi}{\partial y_2^2}(y) + \frac{\partial^2 \phi}{\partial y_3^2}(y)\right),$$

$$(4.19)$$

with boundary conditions on $W_{\bar{y}_1}$

$$\chi_2(y) = 0, \quad \chi_3(y) = 0, \quad \frac{\partial \pi}{\partial n_y^\epsilon} = 0, \quad \frac{\partial \tilde{\phi}}{\partial n_y^\epsilon} = 0, \qquad \text{(adiabatic)}$$

$$\chi_2(y) = 0, \quad \chi_3(y) = 0, \quad \frac{\partial \pi}{\partial n_y^\epsilon} = 0, \quad \phi = -\frac{\partial \rho^0}{\partial x_2}y_2, \quad \text{(isothermal)}$$

and boundary conditions on $\Gamma_{up}^{\bar{y}_1}$

$$\left(\frac{\eta}{\epsilon Re}\left((\nabla \chi_2)^T, (\nabla \chi_3)^T\right) - \pi \mathbb{I}_2\right)n = 0, \quad \nabla \phi \cdot n = 0.$$

Moreover χ_2, χ_3, π and ϕ are periodic in y_3. Note that $\chi_2(y) = \chi_3(y) = 0$, as discussed in Section 4.1.1.

The cell problems are solved using the finite element software package deal.II, cf. [6]. After having computed the solution of the cell problem $\chi_1^{(i)}$ at N selected points $\bar{x}_P^{(i)} \in \Gamma_0$, $i = 1,\ldots,N$, such that $\bar{x}_P^{(i)} = (\bar{x}_{P,1}^{(i)}, 0, 0)^T$, $\bar{x}_{P,1}^{(i)} \in [0.137931, 1]$, the effective constant $\langle \chi_1 \rangle$ is then approximated using $\langle \chi_1 \rangle^*$, i.e. a piecewise linear interpolation of $\{\langle \chi_1^{(i)} \rangle, i = 1,\ldots,N\}$. The corresponding function is plotted in Figure 9 (left), for $N = 6$ points. Observe that for our test cases we can adopt this strategy because the zeroth order solution is invariant in spanwise direction, i.e., the cell function only depends on x_1. In the general case it is not affordable to consider a uniform subdivision of Γ_0 and a parameter dependent solution χ_1 could be determined for example applying model reduction strategies such as the reduced basis method. Figure 9 (right) shows the cell function χ_1 at $\bar{x}_P = (1,0,0)^T$. In particular this picture justifies Hypothesis 2.1 (I) needed in Theorem 3.1, showing that it is numerically satisfied by χ_1. Moreover, the zeroth order solution considered here satisfies the assumptions of Theorem 3.1, thus $\langle \chi_1 \rangle$ is independent of the choice of Γ_{up}.

4.1.3 Isotropic roughness (bump)

In the case of isotropic roughness we need to solve the fully three-dimensional cell problem (4.2), (4.3) and (4.4). As discussed in Section 4.1.1, $\chi_2 = \chi_3 = 0$, thus $\chi = \chi_1 e_1$. As described for longitudinal riblets, the three dimensional cell problem is solved using the finite element software package deal.II, cf. [6], and the effective constants $\langle \chi_1 \rangle^*$ and $\langle \phi \rangle^*$ are plotted in Figure 10.
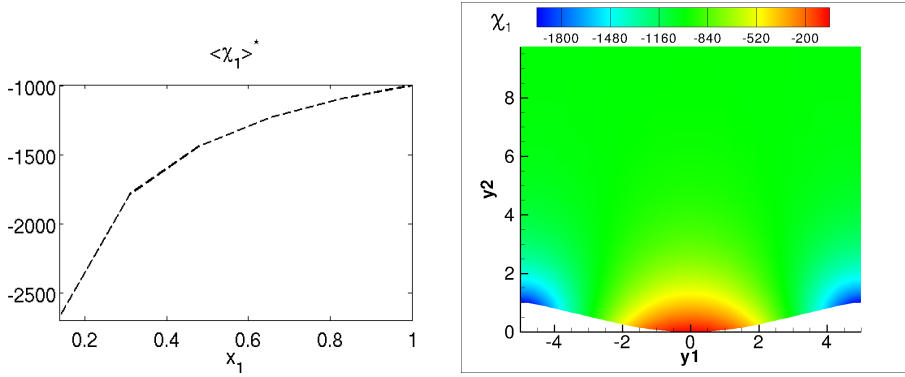
Figure 9: Longitudinal riblets: $\langle \chi_1 \rangle^*$ (left), χ_1 at $\bar{x}_P = (1,0,0)^T$ (right).
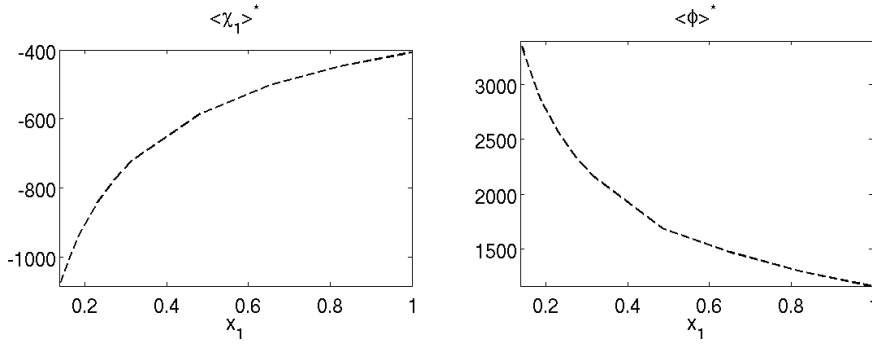
Figure 10: Isotropic roughness: $\langle \chi_1 \rangle^*$ and $\langle \phi \rangle^*$.

Figure 11 shows the cell functions χ_1 and ϕ at $\bar{x}_P = (1 - \epsilon s/2, 0, 0)^T$. Also in this case the Hypothesis 2.1 (I) is satisfied numerically by all cell functions.

4.2 Effective problem

Having solved the cell problem and computed the effective constants $\langle \chi \rangle$ and $\langle \phi \rangle$, we solve now the effective problem (3.31), (3.32) and (3.33a), (3.33b), (3.33c) in case of *implicit boundary conditions* or (3.34a), (3.34b), (3.34c), in case of *explicit boundary conditions*, with the aid of the solver QUADFLOW [9].

The QUADFLOW package solves the compressible Navier-Stokes equations using a cell-centered finite volume method on locally refined grids. Mesh adaptation is based on multiscale analysis [43] instead of classical gradient- or residual-based error estimators. The computational grids are represented by block-structured parametric B-Spline patches [39] to deal with complex geometries. In order to reduce the computational load to a tolerable amount, these tools are
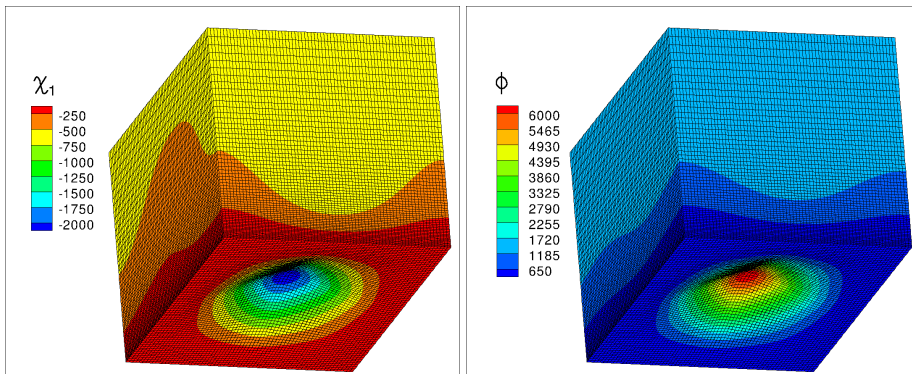
Figure 11: Isotropic roughness: χ_1 and ϕ at $\bar{x}_P = (1 - \epsilon s/2, 0, 0)^T$.

equipped with parallelization techniques based on space-filling curves [11] to run the simulations on distributed memory architectures.

The parameters of the solver used for effective computations and for direct numerical simulations are the same as the ones used in [16] and, thus, are not repeated here.

Computations. For each configuration the effective problem is solved in the effective domain, see Figure 6, with $\sigma = \epsilon$ for both *implicit* and *explicit* boundary conditions. In addition, we compute the solution of the exact problem (3.6), (3.7) on the rough domain, referred to as *direct numerical simulation* (DNS) where the roughness is fully resolved by the discretization. To appropriately resolve the leading edge of the boundary layer, we add an additional region in front of the plate, see Figure 6, where we prescribe symmetry conditions on the lower boundary, i.e.,

$$\rho = \rho_\infty, \quad p = p_\infty, \quad u_1 = u_\infty, \quad \frac{\partial u_j}{\partial n} = 0, j = 2, 3, \quad on \quad \Sigma_{sym}. \tag{4.20}$$

The DNS and the effective solution are computed using different discretizations. To resolve the roughness in the rough domain we locally need a discretization much smaller than ϵ. On the other hand, for the effective problem on the smooth domain a much coarser discretization is sufficient. For comparison we also perform computations of the zeroth order problem that correspond to a flat plate, as in [16, 17].

In the following we consider two test cases: the *isotropic roughness* and the *longitudinal riblets* with isothermal and adiabatic boundary conditions, respectively.

4.2.1 Isotropic roughness

In order to investigate the modeling error we compare the streamwise velocity u_1 and the density ρ, both in spanwise and streamwise direction, cf. Figure 12 and 13, respectively, both computed at Γ_σ.
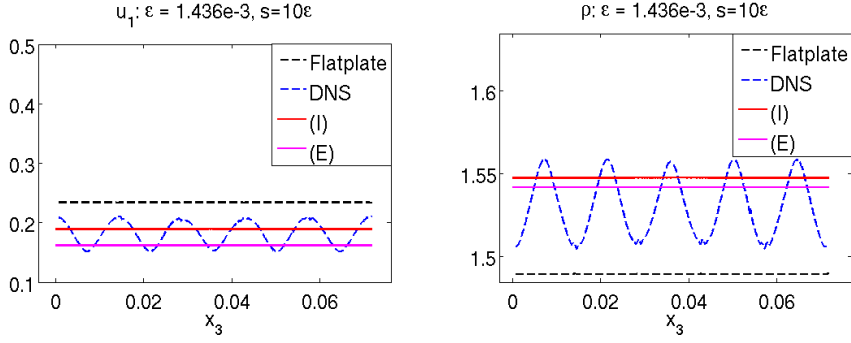
Figure 12: Spanwise direction at Γ_σ ($x_1 = 0.57471$): streamwise velocity u_1 (left) and density ρ (right) both for *implicit*, (I), and *explicit*, (E), method.
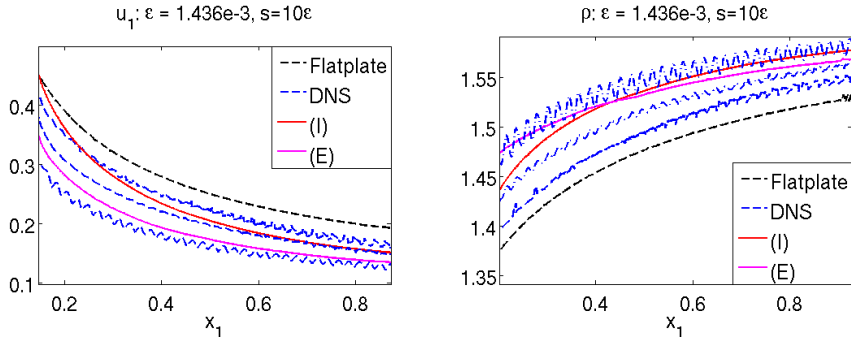
Figure 13: Streamwise direction at Γ_σ: streamwise velocity u_1 (left) and density ρ (right) both for *implicit*, (I), and *explicit*, (E), method.

For the results in streamwise direction we obtain different results for the DNS solution depending on the positions $x_3 = 0.02873, 0.03951, 0.05028$, which correspond to a peak, a middle point and a valley, respectively. All of them are fluctuating around the effective solution, see Figure 13. Both figures show that the effective solution improves the zeroth order approximation of the DNS and the *explicit* method works slightly better than the *implicit* method.

As in [16], in order to compare the effective and the exact solutions in the boundary layer we introduce the wall shear stress τ_w and the wall shear velocity u_τ corresponding to the flat plate

$$\tau_w := \eta_\infty \left.\frac{\partial u_1^0}{\partial x_2}\right|_{\Gamma_0}, \quad u_\tau := \sqrt{\frac{\tau_w}{\rho_\infty}}. \tag{4.21}$$

Then we define the dimensionless wall distance x_2^+ and the dimensionless streamwise velocity u_1^+ by

$$x_2^+ := \frac{u_\tau}{v_\infty} x_2, \quad u_1^+ := \frac{u_1}{u_\tau},$$

where $\nu_\infty := \eta_\infty / \rho_\infty$ denotes the kinematic viscosity coefficient. By means of these quantities the streamwise velocity profile in the boundary layer can be plotted with respect to dimensionless *wall units*, cf. Figure 14 (left). Note that for *all* computations we use the wall shear stress and the wall shear velocity of the *flat plate* to compute the dimensionless wall distance and velocity. The vertical line in the pictures indicate the position of Γ_σ. Note that there is a good qualitative agreement between both effective solutions and the exact solution.
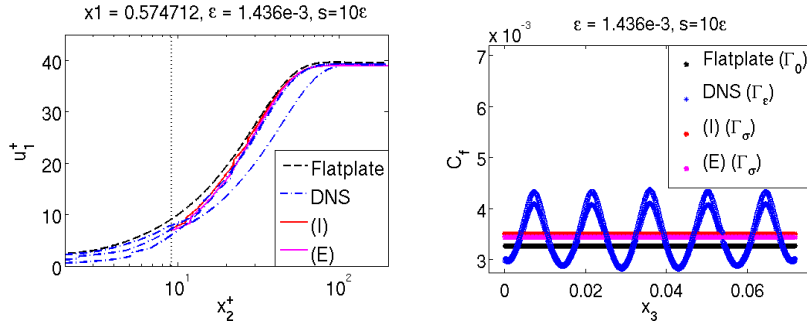
Figure 14: Streamwise velocity in wall normal direction (left) and skin friction coefficient (right).

Finally we consider the skin friction coefficient defined in streamwise direction x_1 in the x_1-x_2-plane

$$c_f = \frac{\tau_w}{0.5 \rho_\infty u_\infty^2},$$

where the wall shear stress τ_w is defined by

$$\tau_w := \eta \left(n_1 \left(t_1 \frac{\partial u_1}{\partial x_1} + t_2 \frac{\partial u_2}{\partial x_1} \right) + n_2 \left(t_1 \frac{\partial u_1}{\partial x_2} + t_2 \frac{\partial u_2}{\partial x_2} \right) \right)$$

with $n = (n_1, n_2, n_3)^T$ the normal vector to the wall and $(t_1, t_2) = (n_2, -n_1)$ if $n_2 \geq 0$ and $(t_1, t_2) = (-n_2, n_1)$ otherwise. In Figure 14 (right) the skin friction is plotted in spanwise direction on Γ_ϵ, Γ_0, Γ_σ in case of the exact problem, the zeroth order problem and the effective problem, respectively. For this test case the *explicit* variant of the boundary conditions seems to give a better estimate for the average of c_f than the *implicit* one.

4.2.2 Longitudinal riblets

Following the analysis of the isothermal test case, we consider now the second configuration, where Neumann boundary conditions are imposed for the density. As before, we compare the streamwise velocity u_1 and the density ρ, both in spanwise and streamwise direction, cf. Figure 15 and 16, respectively. Observe that both the *explicit* and the *implicit* method give a qualitatively better approximation of the velocity u_1 compared with the flat plate solution, and also here the *explicit* method works slightly better. What has to be noted though, is that both approaches do not approximate the density as well as the zeroth order solution, both in streamwise and in spanwise direction.
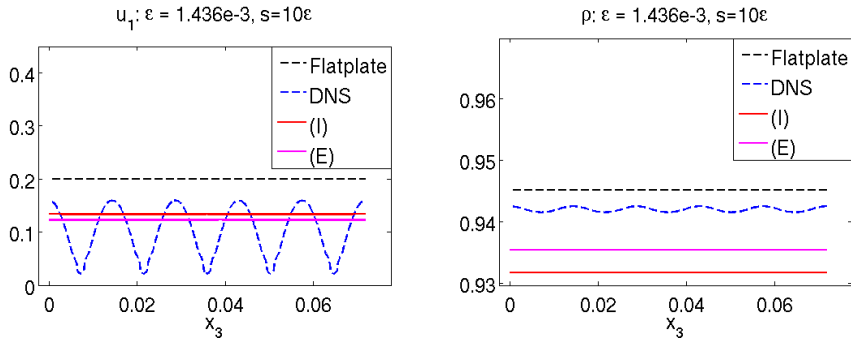
Figure 15: Spanwise direction at Γ_σ ($x_1 = 0.57471$): streamwise velocity u_1 (left) and density ρ (right) both for *implicit*, (I), and *explicit*, (E), method.
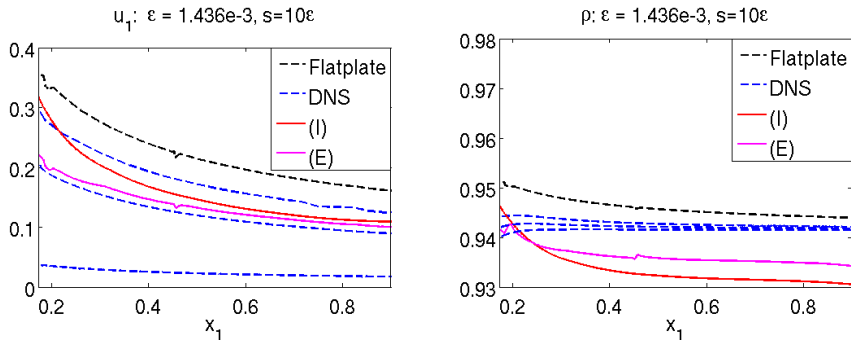
Figure 16: Streamwise direction at Γ_σ: streamwise velocity u_1 (left) and density ρ (right) both for *implicit*, (I), and *explicit*, (E), method.

Figure 17 presents a comparison of the approximations of the wall normal derivative of the density, computed by the solution of the van Driest equations (reference solution), by the flat plate simulation used in *explicit* boundary conditions and by *implicit* boundary conditions, respectively. This picture clearly shows that the approximated quantities we are using in both approaches are fairly accurate. Thus, we conclude that the relatively poor quality of the density approximation is caused by a limitation of the current model. This is also supported by the fact that both the *explicit* and the *implicit* method still provide good approximations for the velocity u_1, where Dirichlet boundary conditions are imposed, cf. Figure 18. A detailed investigation is beyond the scope of this article and will be addressed in future work.
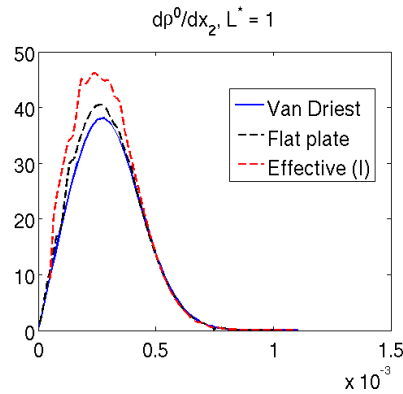
Figure 17: Wall normal derivative of ρ^0: Van Driest solution, flat plate approximation, effective approximation given by *implicit* boundary conditions.
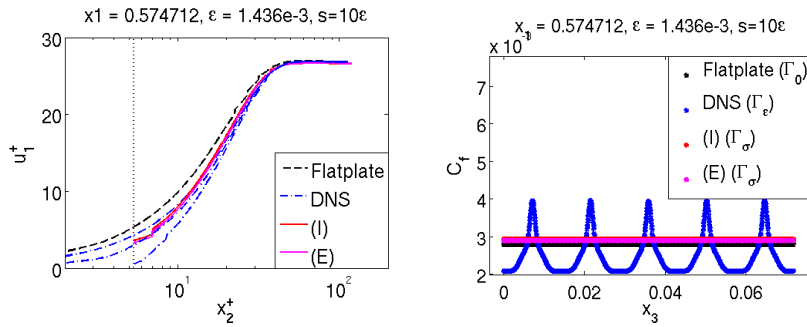
Figure 18: Streamwise velocity in wall normal direction (left) and skin friction coefficient (right).

4.2.3 Efficiency

To estimate the efficiency of the effective solution in comparison with the DNS, we summarize in Table 4.2.3 the number of cells used in the discretizations. We note that the computational load for the DNS is significantly higher, because the roughness requires a much finer grid near the boundary Γ_ϵ than for Γ_σ. The grid is slightly coarser for the flat plate computation than for the effective computations. This is due to the jump in the effective constants of the effective boundary conditions at the leading edge of the virtually smooth roughness region, see Figure 6.

Finally we observe that for both test cases, cf. Sections 4.2.1 and 4.2.2, the *implicit* method gives a slightly worse approximation of the velocity than the *explicit* one. To understand this, we present in Figure 19 the absolute value of the term

$$\epsilon \left(\frac{\partial u_1^0}{\partial x_2}(\bar{x}_P) - \frac{\partial u^{eff}}{\partial x_2}(x) \right),$$ (4.22)

	Longitudinal riblets	Isotropic roughness
DNS	1609144	1148792
(I)	209068	194956
(E)	209278	193388
Flat plate	115520	113980

Table 1: Computational cost.

which enters the expression of the *implicit* error given in equation (2.37).
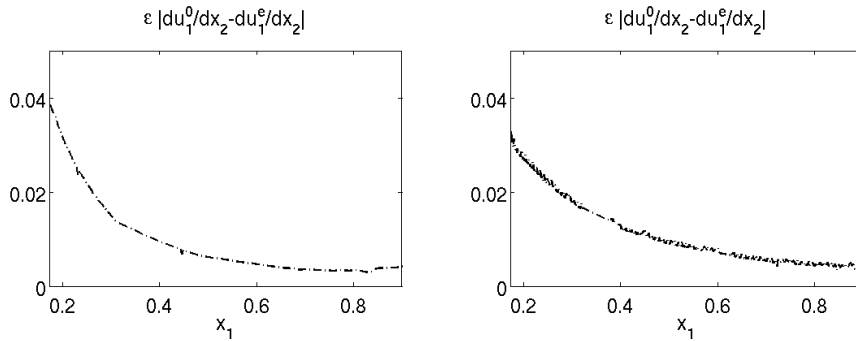
Figure 19: Variation of the absolute value of the term (4.22) in streamwise direction: adiabatic, longitudinal riblets (left); isothermal, isotropic roughness (right).

We observe that the streamwise values where (4.22) is larger in Figure 19, correspond to the values where the approximation error of the velocity is larger in Figures 13 (left) and 16 (left), respectively. For these streamwise values the *explicit* method performs better because the term (4.22) does *not* enter in the *explicit* error formula (2.39).

5 Conclusions

We present a general multidimensional strategy for the derivation of effective boundary conditions to model the effect of a rough surface thus avoiding the resolution of the small scale structures.

When Dirichlet boundary conditions are applied, the effective computations give qualitatively a significantly better approximation of the DNS solution than the flat plate solution, i.e., the up-scaling improves the zeroth order approximation at significantly lower computational cost. Even though the *explicit* method requires a pointwise knowledge of the zeroth order solution, it performs better than the *implicit* strategy.

Although initially inspired by previous work by Achdou et al. [1], Jäger and Mikelic [29, 31], Friedmann et al. [24, 25] and Deolmi et al. [16, 17], the flow regime considered have led us to pursue a different route. Starting point is an asymptotic expansion of the solution of the

exact problem for each flow variable. With the aid of this expansion we derive a so called *cell problem*, which has to be solved at different locations $\bar{x}_P \in \Gamma_0$. Depending on the underlying differential operator all cell functions might be coupled in the cell problem due to nonlinearities. Both adiabatic and isothermal boundary conditions are considered. Moreover, two scenarios are presented for the derivation of effective boundary conditions. In the application considered here, both approaches improve the approximation given by the zeroth order solution, when Dirichlet boundary conditions are imposed.

So far our investigations are restricted to steady state problems. In the future we will also treat time-dependent problems in order to investigate drag reduction at airfoils by means of high-frequency surface waves actuated in spanwise direction. Experimental investigations [34] as well as direct numerical simulations [18, 19] show promising results for a particular frequency range although most of these investigations have been performed for incompressible flows.

Acknowledgments

References

[1] Y. Achdou, O. Pironneau, F. Valentin, "Effective boundary conditions for laminar flows over periodic rough boundaries", *J. Comp. Phys.*, **147**, 187–218, 1998.

[2] Y. Achdou, O. Pironneau, F. Valentin, "New wall laws for unsteady incompressible Navier-Stokes equations", *ECCOMAS 2000*, 2000.

[3] Y. Achdou, P. Le Tallec, F. Valentin, O. Pironneau, "Constructing wall laws with domain decomposition or asymptotic expansion techniques", *Comput. Methods Appl. Mech. Engrg.*, **151**, 215–232, 1998.

[4] Y. Achdou, O. Pironneau, F. Valentin, "Comparison of wall laws for unsteady incompressible Navier-Stokes equations", *First MIT Conference on Computational Fluid and Solid Mechanics, Boston, USA, June 12-15*, 2001.

[5] J.D. Anderson, "Hypersonic and high temperature gas dynamics", *McGraw-Hill Series in Aeronautical and Aerospace Engineering*, 1989.

[6] W. Bangerth, R. Hartmann, G. Kanschat, "deal.II — a general-purpose object-oriented finite element library", *ACM Trans. Math. Softw.*, **33(4)**, 24/1–24/27, 2007.

[7] G.R. Barrenechea, P. Le Tallec, F. Valentin, "New wall laws for the unsteady incompressible Navier-Stokes equations on rough domains", *Mathematical Modeling and Numerical Analysis*, **36**, 177–203, 2002.

[8] A. Basson, D. Gerard-Varet, "Wall laws for fluid flows at a boundary with random roughness", *Commun. Pure Appl. Math.*, **61**, 941–987, 2008.

[9] F. Bramkamp, Ph. Lamby, S. Müller, "An adaptive multiscale finite volume solver for unsteady and steady state flow computations", *J. Comp. Phys.*, **197(2)**, 460–490, 2004.

[10] A. Bensoussan, J.L. Lions, G. Papanicolaou, "Asymptotic analysis for periodic structures", North-Holland, Amsterdam, 1978.

[11] K. Brix, S. Mogosan, S. Müller, G. Schieffer, "Parallelization of multiscale-based grid adaptation using space-filling curves", in Multiresolution and Adaptive Methods for Convection-Dominated Problems, F. Coquel, Y. Maday, S. Müller, M. Postel, Q.H. Tran (eds.), *ESAIM:Proceedings*, **29**, 108–129, 2009.

[12] D. Bresch, V. Milisic, "High order multi-scale wall-laws, Part I: the periodic case", *Quarterly of Applied Mathematics*, **68**, 229–253, 2010.

[13] D. Bresch, V. Milisic, "Towards implicit multi-scale wall-laws", *Comptes Rendus Mathematique*, **346**, 833–838, 2008.

[14] J. Casado-Diaz, E. Fernandez-Cara, J. Simon, "Why viscous fluids adhere to rugose walls: a mathematical explanation", *J. Differential Equations*, **189**, 526–537, 2003.

[15] W. Dahmen, Ch. Plesken, G. Welper "Double greedy algorithms: reduced basis methods for transport dominated problems", *ESAIM: Mathematical Modelling and Numerical Analysis*, **48**(3), 623–663, 2014.

[16] G. Deolmi, W. Dahmen, S. Müller, "Effective boundary conditions for Compressible Flows over Rough Surface", *Math. Models Methods Appl. Sci.*, **25**, 1257–1297, 2015.

[17] G. Deolmi, W. Dahmen, S. Müller, "Effective boundary conditions for Compressible Flows over Rough Surface: Isothermal case", *Proceedings of the XXIV Congress on Differential Equations and Applications - XIV Congress on Applied Mathematics*, ISBN 978-84-9828-527-7, 2015.

[18] Y. Du, G.E. Karniadakis, "Suppressing wall turbulence by means of a transverse traveling wave", *Science* **288**, 1230–1234, 2000.

[19] Y. Du, G.E. Karniadakis, "Drag reduction in wall bounded turbulence via a transverse travelling wave", *J. Fluid. Mech.* **457**, 1–34, 2002.

[20] Y. Efendiev, T.Y. Hou, "Multiscale Finite Element Methods: Theory and Applications", Springer, 2009.

[21] W. E, B. Engquist, "The heterogeneous multiscale methods", *Commun. Math. Sci.* **1(1)**, 87–132, 2003.

[22] W. E, B. Engquist, "The heterogeneous multi-scale method for homogenization problems", in Multiscale Methods in Science and Engineering, 89–110, Lecture Notes Comput. Sci. Eng., Vol. 44, Springer, Berlin, 2005.

[23] E. Friedmann, "Riblets in the viscous sublayer", Inaugural Dissertation, University of Heidelberg, 2005.

[24] E. Friedmann, "The optimal shape of riblets in the viscous sublayer", *J. Math. Fluid Mech.*, **12**, 243–265, 2010.

[25] E. Friedmann, T. Richter, "Optimal microstructures drag reducing mechanism of riblets", *J. Math. Fluid Mech.*, **13**, 429–447, 2011.

[26] K. Iwamoto, K. Fukagata, N. Kasagi, Y. Suzuki, "Friction drag reduction achievable by near-wall turbulence manipulation at high Reynolds numbers", *Physics of Fluids* **17**, 011702, doi:10.1063/1.1827276, 2005.

[27] W. Jäger, A. Mikelic, "On the boundary conditions at the contact interface between a porous medium and a free fluid", *Ann. Scuola Norm. Sup. Pisa Cl. Sci.*, **23**, 403–465, 1996.

[28] W. Jäger, A. Mikelic, "On the interface boundary conditions of Beavers, Joseph and Saffman", *SIAM J. Appl. Math.*, **60**, 1111–1127, 2000.

[29] W. Jäger, A. Mikelic, "On the roughness-induced effective boundary conditions for an incompressible viscous flow", *Journal of Differential Equations*, **170**, 96–122, 2001.

[30] W. Jäger, A. Mikelic, N. Neuss "Asymptotic analysis of the laminar viscous flow over a porous bed",

SIAM J. Sci. Comput., **22**, 2006–2028, 2001.

[31] W. Jäger, A. Mikelic, "Couette flows over a rough boundary and drag reduction", *Commun. Math. Phys.*, **232**, 429–455, 2003.

[32] W. Jäger, A. Mikelic, "On the boundary conditions at the contact interface between a porous medium and a free fluid", *Ann. Scuola Norm. Super. Pisa Cl. Fis. Mat. (IV)*, **23**, 403–465, 1996.

[33] V. Jikov, S. Kozlov, O. Oleinik, "Homogenization of differential operators and integral functionals", Springer, Berlin, 1995.

[34] W.J. Jung, N. Mangiavacchi, R. Akhhavan, "Suppression of turbulence in wall-bounded flows by high frequency spanwise oscillations", *Physics of Fluids* **A 4**, 1605–1607, 1992.

[35] S. Kang, H. Choi, "Active wall motions for skin-friction drag reduction", *Physics of Fluids* **12**, 3301–3304, 2000.

[36] C. Kenig, C. Prange, "Uniform Lipschitz estimates in bumpy half-spaces", *Archive for Rational Mechanics and Analysis*, November 2014.

[37] J. Kevorkian, J.D. Cole, "Perturbation methods in applied mathematics", Applied Mathematical Sciences, Vol. 34. New York-Heidelberg-Berlin: Springer-Verlag, 1981.

[38] J.R. Kweon, R.B. Kellogg, "Regularity of solutions to the Navier-Stokes system for compressible flows on a polygon", *SIAM J. Math. Anal.* **35(6)**, 1451–1485, 2004.

[39] Ph. Lamby, "Parametric multi-block grid generation and application to adaptive flow simulations", Diss. RWTH Aachen, 2007.

[40] A. Madureira, F. Valentin, "Asymptotics of the Poisson problem in domains with curved rough boundaries", *SIAM J. Math. Anal.*, **38**, 1450–1473, 2006/07.

[41] A. Mikelic, "Rough boundaries and wall laws" , in Qualitative properties of solutions to partial differential equations, *Lecture Notes of Necas Center for Mathematical Modeling, edited by E. Feireisl, P. Kaplicky and J. Malek*, **5**, 103–134, 2009.

[42] B. Mohammadi, O. Pironneau, F. Valentin, "Rough boundaries and wall laws", *Int. J. Numer. Meth. Fluids*, **27**, 169–177, 1998.

[43] S. Müller, "Adaptive Multiscale Schemes for Conservation Laws", *Lecture Notes on Computational Science and Engineering*, Vol. 27, first ed., Springer Verlag, 2003.

[44] G. Palmer, "Technical Java", Prentice Hall, 2003.

[45] E. Sanchez-Palencia, "Non-Homogeneous Media and Vibration Theory", Springer, 1980.

[46] H. Schlichting, K. Gersten, "Boundary Layers Theory", Springer, 8th edition, 2000.

[47] M.P. Schultz, K.A. Flack, "The rough-wall turbulent boundary layer from the hydraulically smooth to the fully rough regime", *J. Fluid Mech.*, **580**, 381–405, 2007.

[48] L. Tartar, "The general theory of homogenization. A personalized introduction", Lecture Notes of the Unione Matematica Italiana, 7. Springer-Verlag, Berlin; UMI, Bologna, 2009.

[49] S. Veran, Y. Aspa, M. Quintard, "Effective boundary conditions for rough reactive walls in laminar boundary layers", *Int. J. Heat Mass Transfer*, **52**, 3712–3725, 2009.

[50] M.J. Walsh, in "Viscous drag reduction in boundary layers, Riblets", D.M. Bushnell, J.N. Hefner (eds.), AIAA, New York, NY, 203–261, 1990.

[51] K.-S. Choi, "European drag-reduction research-recent developments and current status", *Fluid Dyn. Res.*, **26**, 325–335, 2000.

[52] D.M. Bushnell, "Aircraft drag reduction — a review", *Proc. Inst. Mech. Eng.*, **217**, 1–18, 2003.

[53] M. Bruse, D.W. Bechert, J.G.T.V. der Hoeven, W. Hage, G. Hoppe, "Near-wall turbulent flows, Experiments with conventional and with novel adjustable drag-reducing surfaces", in R.M. So, C.G. Speziale, B.E. Launder (eds.), Elsevier, Amsterdam, The Netherlands, 719–738, 1993.

[54] D.W. Bechert, M. Bruse, W. Hage, R. Meyer, "Biological surfaces and their technological application — laboratory and flight experiments on drag reduction and separation control", AIAA paper 97-1960,

1997.

[55] M. Itoh, S. Tamano, R. Igushi, K. Yokota, N. Akino, R. Hino, S. Kubo, "Turbulent drag reduction by the seal fur surface", *Phys. Fluids*, **18**, 065102, 2006.

[56] S.-J. Lee, Y.-G. Jang, "Control of flow around a NACA 0012 airfoil with a micro-riblet film", *J. Fluids Struct.*, **20**, 659–672, 2005.

[57] P.R. Viswanath, "Aircraft viscous drag reduction using riblets", *Prog. Aerosp. Sci.*, **38**, 571–600, 2002.

[58] J. Szodruch, "Viscous drag reduction on transport aircraft", AIAA paper 91-0685, 1991.

[59] W.-E. Reif, A. Dinkelacker, "Hydrodynamics of the squamation in fast swimming sharks", *Neues Jahrbuch für Geologie und Paläontologie Abhandlungen*, **164**, 184–187, 1982.